Chronically lowering sympathetic activity protects sympathetic nerves in spleens from aging F344 rats

Sam D. Perez[a], **Brooke Kozic**[b], **Christine Molinaro**[b], **Srinivasan Thyagarajan**[b], **Mark Ghamsary**[c], **Cheri L. Lubahn**[d], **Dianne Lorton**[d,e], and **Denise L. Bellinger**[b,*]

[a]Department of Physiology & Pharmacology, Loma Linda University, School of Medicine, Loma Linda, California, 92350, USA

[b]Department of Human Anatomy and Pathology, Loma Linda University, School of Medicine, Loma Linda, California, 92350, USA

[c]Department of Biostatistics, Loma Linda University, School of Medicine, Loma Linda, California, 92350, USA

[d]Hoover Arthritis Research Center, Banner Sun Health Research Institute, Sun City, AZ 85351, USA

[e]Department of Psychology, Kent State University and the Kent Summa Initiative for Clinical and Translational Research, Summa Health System, Akron, OH 44304, USA

Abstract

In the present study, we investigated how increased sympathetic tone during middle-age affects the splenic sympathetic neurotransmission. Fifteen-month-old F344 rats received rilmenidine (0, 0.5 or 1.5 mg/kg/day, i.p. for 90 days) to lower sympathetic tone. Controls for age were untreated 3 or 18M rats. We report that rilmenidine (1) reduced plasma and splenic norepinephrine concentrations and splenic norepinephrine turnover, and partially reversed the sympathetic nerve loss; and (2) increased β-adrenergic receptor (β-AR) density and β-AR-stimulated cAMP production. Collectively, these findings suggest a protective effect of lowering sympathetic tone on sympathetic nerve integrity, and enhanced sympathetic neurotransmission in secondary immune organs.

Keywords

1. INTRODUCTION

The sympathetic nervous system (SNS) is a homeostatic regulator of cardiovascular, metabolic and immune functions under basal conditions, in the face of acute or chronic

*Corresponding Author and Contact Information: Denise L. Bellinger, Ph.D., Departments of Pathology and Human Anatomy, Loma Linda University School of Medicine, 11021 Campus Street, AH 325, Loma Linda, CA 92350, Tel.: 909-558-7069, Fax: 909-558-0432, dbellinger@llu.edu.

changes in physiological state, and in response to stress. In immune organs, the SNS regulates immune function via tonic release of its major transmitter, norepinephrine (NE) [Bellinger et al., 2008a,b]. NE binds with adrenergic receptors (AR; predominantly β_2) expressed on immunocytes to increase cAMP production [Halper et al., 1984]. The SNS modulates a wide variety of immune measures, and affects the development and progression of immune-mediated diseases [reviewed in Bellinger et al., 2008b].

With aging, basal sympathetic nerve activity (SNA) progressively rises [Docherty, 2002], and SNS responses after activation are exaggerated [McCarty et al., 1997]. The functional significance of hyperactive SNA in immune organs remains unclear and understudied. Presumably, it occurs at the expense of fine control, at the risk of over-stimulating target tissues, and places additional metabolic strain (allostatic load) on all target organs [Goldstein and McEwen, 2002]. Higher SNA can alter immune cell trafficking [Redwine et al., 2003] and host defense [Bellinger et al., 2008b], and may be a risk factor for developing immune-mediated diseases that increase in frequency with advancing age [Bellinger et al., 2008b; Cohen et al, 2001]. Furthermore, the extent to which aging changes in SNS functioning mediate, or contribute to, the aging changes in immune function, i.e. a causal relationship between these two phenomena, remains unknown. This lack of information is due, in part, to a lack of clear understanding of target-specific changes in SNS functioning across age, and the lack of model systems that can reverse the age-induced SNS changes in immune target organs, which is necessary to test this hypothesis *in vivo*.

In aging male F344 rats, sympathetic innervation progressively declines in secondary lymphoid organs [Bellinger et al., 1992, 2008a,b]. Nerve loss resembles a peripheral neuropathy in that nerves recede distally to proximally from their entry sites into the spleen, the hilar region. Nerve loss precedes a significant loss in splenic NE levels, suggesting enhanced NE metabolism as an early compensatory event. This is consistent with a slight, but significant rise in splenic NE concentrations in 10M rats and increased NE turnover between 10 and 15 months. In 24M rats, splenic NE turnover is reduced compared with 8, 10, 12, and 15M rats [Bellinger et al., 2008a]. Age-related splenic denervation is associated with increased lymphocyte responsiveness to β-AR stimulation that is evident in 15M rats [Bellinger et al., 2008a] and altered immune function [Bellinger et al., 2008a,b]. Collectively, our findings indicate that splenocytes from aging F344 male rats respond to changing NE concentration in the local milieu, with compensatory regulation of β-AR expression and cAMP production to affect immune function.

As a first step in developing an aging model for investigating causal relationships between sympathetic and immune dysregulation, we investigated whether heightened splenic SNA during middle age is responsible for splenic NA nerve loss and altered β-AR signaling in splenocytes. In the brain, high catecholamine concentrations are neurotoxic due to increased reactive oxygen species (ROS) from catecholamine degradation [Chinta and Anderson, 2008; Burke et al., 2004]. We propose a similar mechanism affects NA nerve integrity, with consequences for β-AR-mediated signaling in the F344 rat spleen as SNA rises during middle age. In this study, we investigated the effects of chronically reducing SNA centrally during middle age by treatment with rilmenidine (Rilm) on a variety of measures to assess sympathetic integrity and function. Rilm is a centrally acting antihypertensive drug that selectively inhibits sympathoexcitatory cells in the rostroventrolateral medulla (RVLM) [Reis, 1996; Monassier et al., 2004], a brainstem autonomic region that regulates SNA in the spleen [Beluli & Weaver, 1991]. This is the first study to investigate the effects of Rilm, or other drugs in its class, in normotensive rats, with endpoint in immune target organs, and nerve integrity in any organ.

Here, we report that chronic Rilm discontinuously administered during middle age reduced net and splenic SNA, protected splenic NA nerves from age-related damage, and further augmented β-AR-mediated signaling of splenic lymphocytes. Protection of splenic sympathetic nerves supports our hypothesis. Greater β-AR expression and signaling supports reduced NE available to bind with β-AR via reduced SNA and indicates functional β-AR and signaling regulation, an important criterion for developing a model for studying causality between age-related changes in SNS and immune functioning. We conclude that chronic treatment with Rilm during middle age is a strategy for reversing age-related changes in sympathetic neurotransmission in the spleen.

2. METHODS

2.1. Drug Preparation

Rilm dihydrogenase, a centrally acting third generation antihypertensive drug, was a gift from Servier (Suresnes, France). Rilm is stable in solution at room temperature for over 24 hours [Monassier et al., 2004], therefore the drug was prepared once daily prior to the first of two daily injections. Rilm was dissolved in sterile, endotoxin-free, physiologic saline at 0.5 mg/ml or 1.5 mg/ml. Rilm is stable in solution at room temperature for over 24 hours [Monassier et al., 2004]. α-Methyl-$_{DL}$-p-tyrosine methyl ester HCl (αMPT) (Sigma-Aldrich, St. Louis, MO), an inhibitor of tyrosine hydroxylase, the rate-limiting enzyme for the synthesis of NE, was used to determine splenic NE turnover. The αMPT was dissolved in sterile, endotoxin-free, physiologic saline containing 0.1% ascorbic acid at a concentration of 0.2 mg/ml.

2.2. Animals

Seventy-six 15-month-old (15M) male, F344 rats were purchased from the National Institute on Aging (NIA) colony (Harlan Sprague-Dawley; Indianapolis, IN). All animals in the study were housed two per cage in the vivarium at Loma Linda University, given food and water *ad libitum*, and placed on a 12-h-on 12-h-off light schedule. In the animal room, the ambient temperature was maintained at 22 °C, and the humidity ranged between 30-40%. Rats were acclimated to housing conditions for one week, and then were handled daily for one week before the start of the experiment. All animal manipulations and procedures were approved by the institutional animal care and use committee at Loma Linda University prior to the start of the experiments, and followed NIH guidelines on the use and care of animals.

2.3. Study Design

The rats were randomly assigned to one of three treatment groups: low-dose Rilm (Rilm$_{lo}$), high-dose Rilm (Rilm$_{hi}$) or vehicle (Veh-18M) (*n* of 12 per treatment group). Rats were treated with sterile, endotoxin-free saline (Veh-18M) or Rilm (500 or 1.5 mg/ml/kg/day, intraperitoneal (i.p.); Rilm$_{lo}$ or Rilm$_{hi}$, respectively) by twice-daily injections (half the total dose per injection) at 7:30 a.m. and 3:30 p.m. for 90 days. The route of Rilm administration and Rilm$_{lo}$ dose used in this study were based on a previous report by Monassier et al. [2004] demonstrating that chronic treatment (30 days) with this moderate dose of Rilm (250 mg/ml/kg) administered i.p. every twelve hours (i.e., discontinuous) induces the optimum anti-hypertensive action in spontaneously hypertensive rats, when measured at the peak plasma concentration of the drug (30 ng/ml). Discontinuous treatment with 500 mg/kg/day is rapidly eliminated when delivered systemically, so it does not induce receptor desensitization, and it did not affect α_2-AR expression in kidney membrane preparations. The Rilm$_{hi}$ dose was used to determine whether there were dose-response effects and/or whether a dose doubling could further potentiate drug effects on measured parameters. An additional 14 untreated 3M and 18M male F344 rats were obtained from the NIA colony 1 week before the end of the 90-day experiment, and used as controls to assess the potential

effects of the stress of handling and injections. Where no differences were found between vehicle-treated and untreated 18M controls based on Student t-tests ($p<0.05$), the data were collapsed and designated as Ctrl-18M. Body weights were measured prior to starting drug treatment, and then weekly until the end of the experiment. Daily grooming, feeding and drinking behaviors were observed to monitor the general health of each rat. Based on these qualitative observations, Rilm was well tolerated.

For the turnover study, 18M rats treated with vehicle or Rilm for 90 days, and untreated 3M and 18M control rats were randomly assigned to receive either the vehicle diluent for αMPT or αMPT. The αMPT was used to estimate basal rates of NE turnover in the spleen based on the rate of decline in splenic NE concentration after NE synthesis blockade, as previously described [Bellinger et al., 2008a]. At time zero, rats received an injection of αMPT (200 mg/kg, i.p.) or an equivalent volume of sterile, endotoxin-free saline, and sacrificed 6 hr later by decapitation without prior anesthesia.

Peripheral blood and spleens were immediately harvested from each rat. Peripheral blood was collected in 12×75 mm tubes containing 10 mmol/L disodium ethylenediaminetetraacetic acid (EDTA) kept on ice. Blood samples were centrifuged at 1,200 rpm for 10 min. The plasma was collected into microfuge tubes and stored at -80 °C until used for measuring catecholamine concentrations using high-performance liquid chromatography with coulometric detection (HPLC-CD). Spleens were isolated and dissected from each animal then cut in half. Two small pieces were cut cross-sectionally from the central region of one half of the spleen (~3-4 mm thick), frozen on dry ice, and then stored at -80 °C for subsequent measurement of splenic NE concentration and fluorescence histochemistry to localize NA nerves. The other half of the spleen was used to isolate spleen cells for use in cAMP and β-AR binding assays.

Following the collection of plasma and spleen tissue, a gross examination of the brain and all visceral organs was completed for evidence of pathology commonly seen with age, including testicular interstitial cell hyperplasia, severe chronic nephropathy (enlarged and discolored kidneys), bile duct hyperplasia (rough surface of liver), and splenomegaly (enlarged spleen resulting from lymphoma or leukemia originating in the spleen). Rats with any visible lesions, tumors, or overt pathology, were excluded from this study. Three to four rats per chronic treatment group were removed from the study due to overt pathology.

2.4. HPLC-CD for Assessing Catecholamine Levels

Spleen samples were sonicated using a Branson Sonifier 250 in 10 times the volume/wet weight of cold perchloric acid (0.1 M) containing 3,4-dihydroxybenzylamine (DHBA) (10 ng/ml) (Sigma-Aldrich), as an internal standard. Spleen homogenates then were centrifuged at 10,000 rpm for 5 min. The resultant supernatants were transferred to microfilterfuge tubes and centrifuged at 14,000 rpm for 20 min resulting in a minimum of 50 μl of supernatant. Thawed plasma samples (200 μl) were pipetted into 12×75-mm glass test tubes containing 1.0 ml of phosphate buffer (pH 7.0), 1.0 ml of 1.5 M (pH 8.6) Tris buffer and 50 μl DHBA (10 ng/ml). After the tubes were vortexed, 50 mg of acid washed alumina was added, and the tubes were placed on a C10 platform shaker (New Brunswick Scientific, Edison, NJ) for 5 min at 175 rpm. The alumina was then allowed to settle, and the supernatant was aspirated. The alumina was washed by adding double-distilled H_2O, allowing the alumina to settle and then aspirating the supernatant for a total of 3 times. At the of the 3rd, wash, the alumina was resuspended in double-distilled H_2O and the resulting slurry was transferred in a sample tube of a microfilterfuge tube and centrifuged for 2 min at 9,000 rpm. Following centrifugation, the sample tube containing the alumna was transferred onto a new receiver tube. Two hundred microliters of 0.1 M $HClO_4$ were added to the alumina. The catecholamines were eluted by centrifuging the microfilterfuge tube for 2 min at 9,000 rpm

and the eluate was collected. NE and DA concentrations were determined using HPLC-CD using a CouloChem III HPLC System (ESA, Chelmsford, MA) and an ESA Model 542 autosampler. The mobile phase was delivered at a flow rate of 1.0 ml/min through a Resolve C18 reverse phase 5-μm, 8×100-mm Radial-Pak analytical column (Canton, Massachusetts) using an ESA Model 582 solvent delivery module. The potentials of the guard cell and two detecting cells of the ESA CouleChem III coulometric detector cell system were set at 400 mV, 350 mV, and -350 mV, respectively. The signal from the detector was recorded and the peak heights and area under the curves were analyzed using EZChrom Elite Software (Scientific Software Inc. Pleasanton, CA).

2.5. Splenic NE Turnover

To determine splenic NE turnover, NE decay was estimated using a model in which the rate of NE reduction following synthesis blockade is defined by a single mathematical factor to which steady-state kinetics can be applied, as previous described [Bellinger et al., 2008a]. According to this model the concentration of NE is dependent on the rate of synthesis with the following relationship: $\text{Log[NE]} = \text{Log[NE]}_o - 0.434kt$, where $[\text{NE}]_o$ is the initial concentration of NE and k is the fraction of NE concentration formed or lost per unit time. The k of NE was calculated by least-square linear regression of the Log[NE] vs. time. To determine the rate constant, turnover time and turnover rate for NE in the spleen, the log of NE (Log[NE]) concentration was plotted versus the time following synthesis blockade. Linear regression analysis of the Log[NE] vs. time relationship was performed using individual data points obtained at 0 and 6 hr after tyrosine hydroxylase inhibition. The slope (m) and standard error of the regression coefficient (Ser) were computed by the least squares method. The rate constant for NE disappearance (kNE defined as m/0.434), NE turnover time (1/kNE), and NE turnover rate ($[\text{NE}]_o \times kNE$) were calculated as described. The standard error of the turnover rate and the turnover time was calculated from the variance of the regression slope and the variance of $[\text{NE}]_o$ according to the delta method, using the following equation:

$$\text{Variance } k(\text{NE})_o = k^2 \text{var}(\text{NE}_o) + [\text{NEo}]^2 \text{var}(k) + 2k\text{NE}_o * \text{Covariance } k, \text{NE}_o.$$

2.6. Fluorescence Histochemistry for Catecholamines

A modification of the glyoxylic acid condensation method (SPG method) of histofluorescence for catecholamines was used to visualize sympathetic nerves in fresh frozen spleen tissue from F344 rats, as previously described [Bellinger et al., 1992]. From each animal, spleen blocks from the hilus (the site of blood vessel and nerve entry into the spleen) and regions distal to the hilus were mounted onto chucks with OCT compound, and 16 μm cross-sections were cut using a cryostat set at -20 °C. Sections were thaw-mounted onto glass slides, and dipped in a 0.2 M potassium phosphate solution containing 1% glyoxylic acid and 0.2 M sucrose (pH 7.4). The slides were air-dried under a direct stream of cool air for 15 min, several drops of mineral oil placed onto each section, and the slides placed on a heat-conducting copper plate in an oven at 95 °C for 2.5 min. Excess oil was drained from the slides, and the slides were coverslipped using 2 drops of fresh mineral oil. Catecholamine fluorescence was visualized using a Zeiss Axiomat fluorescence microscope equipped with epi-illumination accessories, and using a 395- to 440-nm excitation filter. Color images were captured with an Olympus image high-resolution CCD video capture system.

2.7. Spleen Cell Preparation

At sacrifice, one-half of the spleen was placed into a stomacher bag containing 10 ml Hank's balanced salt solution (HBSS) (Mediatech Inc., Manassas, VA) containing 0.035% sodium bicarbonate (Sigma-Aldrich, St. Louis, MO) and 25 mM HEPES (Mediatech Inc., Manassas, VA) and dissociated using a stomacher Lab-Blender (Tekmar Co., Cincinnati, OH). Cell suspensions were passed through 100 μm cell strainers (BD Biosciences Discovery Labware, Bedford, MA) to remove large aggregates, then centrifuged, and resuspended in fresh HBSS. Red blood cells were removed from spleen cell suspensions by layering over Histopaque 1077 (Sigma-Aldrich), and centrifuging at $400 \times g$ for 30 min at room temperature. Cells at the interface between Histopaque and HBSS were removed and washed three times in HBSS. Cells were counted using a Coulter Counter (Coulter Instruments, Hialeah, FL), and then resuspended to 2×10^6 cell/ml in HBSS. Spleen cell suspensions were used for β-AR binding and cAMP assays after adjusting to the appropriate cell concentrations for each assay.

2.8. β-AR Binding Assays

The experimental design and number parameters evaluated in this study limited our ability to carry out binding studies in all treatment groups. Therefore, radioligand binding studies were performed on whole spleen cells from Veh-18M and $Rilm_{lo}$-treated rats (n of 6 per group) using the ligand (-)[^{125}I]cyanopindolol ([^{125}I]CYP), a β-AR antagonist with equal affinity for the β_1- and β_2-AR subclasses. $Rilm_{lo}$-treated rats were chosen for binding studies based on functional data from Monassier et al [2004], as described above. Spleen cells used for β-AR binding assays were resuspended to 5×10^6 cells/ml. [^{125}I]CYP (2200 Ci/mMole) was purchased from GE Healthcare (Piscataway, NJ), and diluted in 1% ethanol, 5 mM HCl, and 0.2% bovine serum albumin (BSA). Assays were performed in duplicate in 13×100-mm polypropylene tubes containing 1×10^6 spleen cells with 8 concentrations of [^{125}I]CYP ranging from 15.8-333 pM. Nonspecific binding was determined using parallel assays incubated in the presence of 10^{-6} M CGP-12177, a hydrophilic β-AR antagonist (Sigma-Aldrich). Tubes were incubated at 37 °C for 60 min in a shaking water bath (100 oscillation/min) to ensure that equilibrium was reached. The reaction was terminated by adding 3 ml of ice cold hypotonic buffer (3.8 mM KH_2PO_4, 16.2 mM K_2HPO_4, 4 mM $MnSO_4$) for 20 min to lyse the cells. The reaction mixture was filtered using a cell harvester (Brandel Corp., Gaithersburg, MD) and bound radioactivity collected on Whatman fiberglass filters (GF/B) (Brandel Corp., Gaithersburg, MD). Filters were washed with 16 ml (4×4 ml) of ice-cold Tris-EGTA buffer to remove the unbound radioligand. Filters were removed, placed in 12×75-mm tubes, and counted in a Wallac 1470 Wizard gamma counter (Long Island, Port Jefferson, NY) at 82% efficiency.

2.9. β-AR-Stimulated cAMP Production in Spleen Cells

Spleen cells (1×10^6) were incubated with 100 μl HBSS containing 100 μM isobutylmethylxanthine (IBMX; Sigma-Aldrich) and 0.1% BSA (EMD Chemicals, Gibbstown, NJ) (IBMX) in 12×75-mm polystyrene tubes (Thermo Fisher Scientific, Pittsburgh, PA) for 20 min at 37 °C in a shaking water bath. Spleen cells were then treated with 1 ml 10^{-5} M isoproterenol (Sigma-Aldrich) for 10 min at 37 °C. The reaction was quenched by adding 2 ml ice-cold IBMX. The tubes were centrifuged for 8 min at 1,800 rpm, and the supernatants discarded. The pellets were reconstituted with 0.5 ml of a 50 mM sodium acetate buffer. The tubes were then exposed to two cycles of boiling and freezing to lyse the cells. The cellular debris was removed by centrifugation (1,800 rpm for 8 min), the supernatants were collected into microfuge tubes, and then stored at -80 °C until assayed for cAMP. cAMP levels were determined in triplicate using a commercially available enzyme immunoassay (EIA) Kit (GE Healthcare, Piscataway, NJ) using the acetylation protocol for highest test sensitivity (lower detection limit of 14 pg/ml) according to the manufacturer's

instructions. The optical density of the samples was determined using a plate reader set at 450 nm.

2.10. Data Analysis

Body and Spleen Weights—Body and spleen weights were expressed in g ± standard error of the mean (SEM). Spleen weights were also expressed as a percentage of body weight ± SEM. These data were analyzed by one-way analysis of variance (ANOVA) with Bonferroni post-hoc testing for significant ANOVA ($p<0.05$).

HPLC-CD Determination of Plasma and Splenic Catecholamine Levels, and NE Turnover—Splenic and plasma catecholamine concentrations were determined based on standards of known concentrations of NE, DA, and EPI, and expressed as a mean ± SEM in ng per g tissue wet weight and ng/ml plasma, respectively. Since age and Rilm treatment affect spleen weight, total NE and DA content were also estimated based on NE concentrations/mg wet weight and whole spleen weight, and expressed as a mean ± SEM in ng/whole spleen. Similarly, turnover rate and time were expressed as means ± SEM in ng/g/h and h, respectively. All these data were analyzed using one-way ANOVA with Bonferroni post-hoc testing for significant ANOVA ($p<0.05$). Splenic NE and DA levels (concentration and total content) were correlated with spleen weight using linear regression analysis and the statistical software, Prism® 4 (GraphPad, San Diego, CA).

Morphometric Analysis of Nerve Density—The density of sympathetic innervation of the white pulp from hilar and distal regions was estimated using the spleens of six rats from each treatment group. The white pulp was chosen for analysis, because the majority of NA nerves in the spleen reside in this compartment [Bellinger et al., 2008b]. Four randomly selected white pulps from each of the six rats per treatment group were used for analysis. Each white pulp area assessed was from a different spleen section near the hilar region or distal to the hilus. White pulps were photographed at a magnification of 200X. The criteria for selecting the white pulps for analysis were that (1) there was only one central arteriole in the white pulp; (2) the size of the central arteriole were comparable across all samples (80-100 μm across the largest diameter of the vessel) and (3) the arteriole was cut in true cross section [Bellinger et al., 2002]. Quantitation of the mean area of NA nerves in the splenic white pulp was performed using Image-Pro Plus® imaging software (version 5.0; Media Cybernetics, Bethesda, MD). Using this software, the area of NA nerves in the total region of interest (ROI) within the white pulp was determined by the number of pixels containing NA nerve profiles in each image, based on size and color. The number of positive pixels was divided by the total number of pixels in the ROI then multiplied by 100 to calculate the % area of NA nerve profiles in each image. The mean % area of NA nerves was determined by averaging the % NA nerve area in four white pulps from each animal, and then these means were averaged within each treatment group. Data were expressed as a mean of a mean ± SEM for each treatment group. Differences in mean % area of NA nerves among the treatment groups were analyzed using a one-way ANOVA ($p<0.05$) followed by Bonferroni post-hoc analysis.

Radioligand Binding—Specific binding was defined as the difference between binding of the radioligand at each concentration in the absence and in the presence of (-)CGP-12177. Nonspecific binding ranged from 10-20% of total binding. Receptor density (B_{max}) and affinity (K_D) were determined using an iterative nonlinear regression curve fitting program, Prism® 4, to a model of a single class of homogenous binding sites. Data were transformed into a linear form by Scatchard analysis. The lines of best fit were generated using the B_{max} and K_D to determine the X and Y axis intercepts. The maximal number of binding sites per cell was calculated based on simple stoichiometric assumptions (1 molecule of ligand

bindings to 1 receptor site), expressed as sites/cell. Differences in mean K_D and B_{max} between groups were determined using one-way ANOVAs ($p<0.05$) followed by Bonferroni post-hoc analysis.

β-AR-Stimulated cAMP Production—β-AR-stimulated cAMP production was expressed as means ± SEM in fmol/2×10^6 cells/10 min. These data were analyzed using a one-way ANOVA ($p<0.05$) with Bonferroni posthoc testing.

3. RESULTS

3.1. Rilm Alters Body and Spleen Weights

F344 rats appeared to tolerate Rilm or vehicle treatment well as all rats were observed to eat, drink, and groom. Prior to beginning the experiment, body weights between treatment groups were comparable (Fig. 1A). Mean body weights from all Rilm treatment groups receiving twice-daily injections, were slightly reduced, but were not significantly different from initial body weights over the 90-day period or compared with body weights of vehicle-treated rats. Mean body weights from vehicle- and drug-treated groups at 12 weeks were significantly (***, $p<0.001$) lower than Ctrl-18M rats (Fig. 1A).

Spleen weights (Fig. 1B) were significantly greater (†††, $p<0.001$) in all 18M treatment groups compared with Ctrl-3M rats, and greater in the Rilm$_{hi}$-treated rats compared with Rilm$_{lo}$ and Ctrl-18M rats (***, $p<0.001$). There were no differences in spleen weights between Veh-18M and untreated-18M, so the data were collapsed (collectively, Ctrl-18M). Similarly, no differences in spleen weights between Rilm$_{lo}$-treated rats and Crtl-18M rats were observed. Mean spleen weight per body weight (Fig. 1C) was significantly greater in rats treated with Rilm$_{hi}$ compared with all other treatment groups (Ctrl-3M: ***, $p<0.001$; Ctrl-18M: *, $p<0.05$; Rilm$_{lo}$: **, $p<0.01$).

3.2. Rilm Reduces Plasma NE Concentrations, but not EPI Concentrations

Mean plasma NE and EPI concentrations (Figs. 2A and 2B, respectively) were similar at 3 and 18 months of age (Ctrl-3M vs. Ctrl-18M). Chronic Rilm$_{lo}$ or Rilm$_{hi}$ treatment significantly reduced plasma NE concentrations (Fig. 2A) compared with Crtl-3M (*, $p<0.05$) and Crtl-18M (**, $p<0.01$) control values. Plasma NE levels in Rilm$_{lo}$- and Rilm$_{hi}$-treated rats were 35% and 29% lower than the controls, respectively. Rilm had no effect on mean plasma EPI concentrations (Fig. 2B).

3.3. Rilm Partially Reverses the Age-Related Decline in Splenic NA Innervation

In Ctrl-3M rats, NA nerves form a dense plexus surrounding the central arteriole in the splenic white pulp in the hilar region (Fig. 3A). Linear, varicose fibers extend from this vascular plexus into the surrounding periarteriolar lymphatic sheath (PALS), a predominantly T cell compartment. In contrast, while the NA nerves display a similar distribution in the white pulp, the density of fluorescent profiles was markedly reduced in this compartment in the Ctrl-18M rats (Fig. 3B). Rilm$_{lo}$ or Rilm$_{hi}$ treatment (Figs. 3C and 3D) increased the fluorescence intensity and density of NA nerve fibers associated with the central arteriole and in the surrounding PALS compared with the Ctrl-18M rats, an effect that appears to be augmented with Rilm$_{lo}$ treatment.

Morphometric analysis confirmed the age-related decline in splenic NA nerve area in the hilar region and partial restoration of nerve loss with Rilm treatment (Fig. 3E). Mean splenic NA nerve density in Ctrl-18M rats declined to 62.3% of Crtl-3M values (***, $p<0.001$). Treatment of rats with Rilm$_{lo}$ or Rilm$_{hi}$ significantly increased the density of NA fibers around the central artery and in the white pulp of the spleen by 60.0% and 44.5%,

respectively (**, $p<0.001$ and *, $p<0.05$, respectively). Despite the dramatic drug-induced increase in mean NA nerve area with $Rilm_{lo}$- or $Rilm_{hi}$ treatment, values remained significantly lower than values in Ctrl-3M rats ($p<0.05$ and $p<0.01$, respectively).

In the distal region, the effects of age and Rilm treatment on nerve density in the white pulp were similar to findings in the hilar region, although the size of the white pulps and diameter of central arterioles appear smaller than in the hilus where the splenic artery and associated sympathetic nerves enter the spleen (Figs. 4A-D). Also like the hilar region, the distribution of NA nerves in the white pulp in this region was not affected by Rilm treatment. Qualitatively, the abundance of NA nerves was reduced along the central arteriole and the surrounding white pulp in Ctrl-18M rats (Fig. 4B) compared with Ctrl-3M rats (Fig. 4A). Both $Rilm_{lo}$ and $Rilm_{hi}$ appeared to dose-dependently increased in the presence of NA nerve fibers associated with the arteriole and in the periarteriolar lymphatic sheath compared with Ctrl-18M rats. Findings from morphometric analysis (Fig. 4E) were consistent with qualitative observations, demonstrating a 66% drop in nerve density at 18 months of age compared with young controls (***, $p<0.001$), and $Rilm_{lo}$ or $Rilm_{hi}$ treatment reversed the aging effect by 91% or 54% (vs. Ctrl-18M: **, $p<0.01$ or **T**, $p<0.1$ (trend), respectively). However, drug treatment did not totally restore nerve density to young adult levels as nerve densities were 35% or 47% lower with $Rilm_{lo}$ or $Rilm_{hi}$ treatment compared with young adult controls (††, $p<0.01$ or †††, $p<0.001$, respectively) (Fig. 4E).

3.4. Rilm Affects Splenic NE and DA Content and Concentration

The mean total splenic NE concentration (Fig. 5A) was lower in Ctrl-18M and $Rilm_{hi}$ than in Ctrl-3M rats (***, $p<0.001$). NE concentration in spleens from $Rilm_{hi}$-treated rats also fell significantly compared with levels found in Ctrl-18M- and $Rilm_{lo}$-treated rats (*, $p<0.05$ and **, $p<0.01$, respectively). A significant age-related decline in mean total splenic NE content (Fig. 5B) was observed, such that Ctrl-18M rats displayed lower values than Ctrl-3M (*, $p<0.05$). The mean splenic NE content in $Rilm_{lo}$-treated rats was similar to values obtained for Crtl-18M, but tended to be lower than in Ctrl-3M rats (**T**, $p<0.1$) (Fig. 5B). No difference in mean splenic NE content was observed between the $Rilm_{lo}$ and Ctrl-18M rats. Mean total NE content in the spleen was reduced in $Rilm_{hi}$-treated rats compared with Ctrl-3M (***, $p<0.001$), but did not differ significantly from the Ctrl-18M or $Rilm_{lo}$ groups. Regression analyses revealed a decrease in NE levels as spleen weight increases (Figs. 5C and 5D). Both splenic NE concentration and total content were significantly correlated with spleen weight, with the former having a greater effect ($p<0.001$ and $p<0.01$, respectively).

There was no effect of either age or low dose drug treatment on splenic DA concentration (Fig. 6A). However, $Rilm_{hi}$ significantly raised DA levels in the spleen to approximately 30%, 34% or 54% of Ctrl-3M, Ctrl-18M, or $Rilm_{lo}$, respectively (*, $p<0.05$; *, $p<0.05$, or **, $p<0.01$, respectively) (Fig. 6A). Similarly, $Rilm_{hi}$-treated rats had a higher total splenic DA content (Fig. 6B) than Ctrl-3M (*, $p<0.05$), Ctrl-18M (*, $p<0.05$) and $Rilm_{lo}$ (**, $p<0.01$) treatment groups. There were no differences between the other treatment groups. In contrast to NE in the spleen, there was no correlation between either DA concentration or total content in the spleen and spleen weight (Figs. 6 C or 6D, respectively).

3.5. Rilm Treatment Reduced Splenic NE Turnover

Intraperitoneal injection of αMPT reduced mean concentrations of NE in spleens from Ctrl-18M and $Rilm_{lo}$ or $Rilm_{hi}$ treatment groups during the 6-h period after NE synthesis blockade (Fig. 7 and Table 1). The rate of decline in splenic NE concentration was greatest in Ctrl-18M rats and lowest in the $Rilm_{hi}$ treatment group (Fig. 7). Calculated NE turnover rate, based on the slopes of the lines (Table 1) and regression analysis revealed a 32.6% and

81.7% decline in splenic NE concentration 6 h after NE synthesis blockade with $Rilm_{lo}$- or $Rilm_{hi}$-18M treatment compared with the Ctrl-18M group, respectively. Turnover rate at 18M in this study was approximately 3.6-fold higher than in 15M rats based on a previous report from our laboratory [Bellinger et al., 2008a], and $Rilm_{lo}$ or $Rilm_{hi}$ turnover rates were 2.4-fold higher or 0.7-fold lower than reported in 15M rats, respectively (Table 1). Rilm dose-dependently increased turnover time (the time required to synthesize the steady-state pool of splenic NE) compared with Ctrl-18M by the 90th day of treatment (Table 1). There was no significant difference in NE content between age-matched and vehicle-treated controls 6 h post-treatment and rats treated with vehicle or αMPT at time 0 (data not shown).

3.6. Rilm Treatment Alters β-AR Binding and Affinity in Spleen Cells

Figs. 8A and 8B show saturation isotherms obtained from saturation binding experiments of splenocytes obtained from Veh-18M- and $Rilm_{lo}$-treated rats, respectively. Binding of the radioligand was rapid, saturable, and of high affinity in both treatment groups. Specific binding was greater than 90% of the total binding at near saturating radioligand concentrations. The Scatchard plots shown in the insets of Figs. 8A and 8B, indicated similar K_D values between the two treatment groups (similar slope of the line), but the B_{max} was greater in rats treated with $Rilm_{lo}$. In spleen cells from rats with $Rilm_{lo}$ treatment, the mean B_{max} was significantly higher (22%, *, $p<0.05$) compared with Veh-18M rats (Fig. 9A), but there was no significant difference in the mean K_D between these treatment groups (Fig. 9B). Spleen cells from rats with Veh-18M and $Rilm_{lo}$ treatment expressed approximately 759 and 1080 sites/cell, respectively (95% confidence intervals were 672-846 for Veh-18M vs. 861-1298 for $Rilm_{lo}$).

3.7. Rilm Treatment and β-AR-Stimulated cAMP Production in Spleen Cells

Isoproterenol-stimulated cAMP production in spleen cells rose significantly (35%; *, $p<0.05$) in Ctrl-18M compared with Ctrl-3M rats (Fig. 10). Chronic $Rilm_{lo}$ or $Rilm_{hi}$ treatment further augmented isoproterenol-induced production of cAMP (***, $p<0.001$ and **, $p<0.01$, respectively) compared with Ctrl-3M rats. In addition, there was a respective 36% (†, $p<0.05$) and 23% increase in cAMP production in the $Rilm_{lo}$- or $Rilm_{hi}$-treated compared with Ctrl-18M rats.

3. DISCUSSION

There are several salient and novel findings in this study. First, in normotensive rats [McCarty, 1985], reduced splenic NE turnover and plasma NA concentrations indicate that chronic Rilm treatment dose-dependently reduced splenic and whole body SNA, respectively. Next, chronic Rilm treatment dose-dependently protected NA nerves from age-related damage in the white pulp in both hilar and distal regions, indicating that age-related loss of sympathetic nerves can be prevented. Collectively, these two findings support our hypothesis that elevated sympathetic tone in the aging spleen causes sympathetic nerve loss. Finally, Rilm augmented β-AR signaling in splenic lymphocytes. This finding neither supports nor refutes our hypothesis, but can be explained by the drugs action on splenic SNA. Reduced SNA reduces NE availability and consequently ligand-receptor interactions, which causes a compensatory increase in β-AR expression, consistent with our findings.

The RVLM regulates SNA in a number of organs [McAllen et al., 1995], including the spleen [Beluli and Weaver, 1991]. The Rilm-induced reduction in splenic and net SNA is consistent with its stimulatory action on sympathoexcitatory neurons in the RVLM via interaction with IR_1 (and α_2-AR) (Fig. 11A) [Bruban et al., 2001]. Activation of these RVLM neurons dampens the firing rate of postganglionic NA nerves via inhibition of

preganglionic neurons in the intermediolateral cell column (IML) in the spinal cord (Fig 11A). Not all of our drug effects may be mediated centrally. IR_1 are expressed in other sympathetic target tissues [Dardonville and Rozas, 2004; Dontenwill et al., 1999], but have not been reported in the spleen. Also, imidazoline binding sites are presynaptically expressed on NA nerves in other visceral organs and can block NE release [Göthert et al., 1999]. However, α_2-AR are expressed presynaptically in sympathetic nerves [Docherty, 2002] and splenic macrophages [Spengler et al., 1990]. Effects of Rilm via presynaptic α_2-AR would be expected to augment its central effect via presynaptic inhibition of NE release [Szabo, 2002]. It is unlikely that drug interactions with α_2-AR on immunocytes contribute to β-AR-mediated cAMP production in splenic lymphocytes, as baseline cAMP levels were not affected, α_2-AR or IR_1 have not been reported on splenocytes, and both receptor types signal through different intracellular pathways [Ernsberger, 1999].

The drug-induced reduction in plasma NE levels, which reflect NE spillover into the blood after its release from NA nerves, is consistent with reduced net SNA in other studies [Monassier et al., 2004; Burke et al., 2009]. The magnitude of reduced plasma NE levels in this study is comparable to both human and animal studies using Rilm as an antihypertensive agent [Esler et al., 2004; Monassier et al., 2004]. The low doses of Rilm in this study did not change plasma EPI levels, consistent with a study in hypertensive patients [Esler et al., 2004]. These findings indicate that the SNS and the sympathoadrenal-medullary (SAM) axis are differentially regulated by autonomic centers in the brainstem, and the SNS can be functionally disconnected from the SAM axis.

The age-related loss in splenic NE concentration and content and NA nerve loss in aging is consistent with our previous findings [Bellinger et al., 2008a]. NA nerve loss contributes to reduced NE in the spleen, but other aging-related mechanisms likely play a role, such as reduced NE reuptake [Docherty, 2002], increased NE release and/or greater degradation (Fig. 11B). Tissue NE levels are normally stable even under extreme conditions, such as stress [Del Rey et al., 1982]. Tight regulation of tissue NE levels explains unaltered static splenic NE concentration and content with $Rilm_{lo}$ treatment and in control groups, but at a lower set point in old rats. Precise regulation of NE reuptake, and enzymes that synthesize and catabolize NE, assures stable tissue NE concentrations (Fig. 11B). Altered splenic NE and DA concentrations with $Rilm_{hi}$ suggest dysregulation of NE homeostasis. Greater ROS from catabolized DA after release could explain the lower nerve sparing ability of $Rilm_{hi}$, consistent with findings centrally in DA neurons [Chinta and Anderson, 2008]. While altered splenic NE levels provide information about homeostatic dysregulation, unaltered levels are inconclusive, and may mask altered SNS functioning. With synthesis blockade, Rilm dose-dependently reduced the rate of NE degradation and increased turnover time, consistent with reduced NE utilization and supporting reduction of SNA by Rilm.

$Rilm_{hi}$, but not $Rilm_{lo}$, reduced splenic NE concentration and content compared with age-matched controls. These data indicated NE synthesis did not keep pace with NE utilization in the $Rilm_{hi}$ treatment group, despite reduced turnover at both drug doses. In aging, higher SNA increases TH activity [Parrish et al., 2008; Morgenroth et al., 1974], an effect reduced by Rilm (Fig. 11B). Our finding of greater splenic DA levels with $Rilm_{hi}$ also supports reduced TH activity via end product inhibition (Fig. 11B) [Flatmark et al., 2000]. High vesicular DA concentrations drive small rates of DA into the cytosol [Reed et al., 2010; Wallace, 2007] to inhibit TH activity. Additionally, the drug-induced SNA decrease may affect TH phosphorylation, critical for its activity and the primary mechanism for maintaining tissue NE levels after secretion [Dunkley et al., 2004; Kumer and Vrana, 1996]. Still, high vesicular DA should drive DA conversion to NE by dopamine-β-hydroxylase (DBH) downstream of TH (Fig. 11B). Thus, reduced splenic NE levels with $Rilm_{hi}$ suggests reduced DBH expression or activity (Fig. 11B). Additionally, (1) increased and reduced NE

and DA release, respectively; (2) reduced vesicular DA transport; and/or (3) altered degradation of NE and DA may contribute to our findings.

Preservation of NA nerves in hilar and distal regions with Rilm supports our hypothesis that SNA during middle-age contributes to nerve loss, an effect that is greater with $Rilm_{lo}$. Our findings are consistent with reports in aging rats that splenic NA nerves remain plastic [ThyagaRajan et al., 2000]. This supports the feasibility for developing a model to investigate causality between aging SNS and immune functional changes. Greater protection may be afforded by earlier treatment, since altered splenic architecture and immune cell subsets occur before 15 months of age [Bellinger et al., 1992]. Also, combined Rilm treatment with trophic factors (i.e., NGF) may potentiate the Rilm effect. Here neuroprotection occurred without reversal of splenic NE levels. However, splenic NE levels may be restored once $Rilm_{lo}$ is withheld, because it appears that synthetic regulatory mechanisms are intact in the aging spleen.

We propose that increased neurotoxic ROS from CA breakdown destroys splenic NA nerves (Fig. 11B). This mechanism of nerve loss occurs in other CA neurons with increased activity, including NA nerves in cerebral vessels [Cowen and Thrasivoulou, 1990], and locus coeruleus and nigrostriatal neurons [Jinsmaa et al., 2009; Chen et al., 2003]. Changes in the microenvironment of the aging spleen may also contribute to nerve loss via intracellular calcium dysregulation [Stirling et al., 2010; Tsai et al., 1998], altered splenocyte subset percentages/absolute numbers [Jiang et al., 1992; Wong et al., 2010; Banerjee et al., 2000; Fló and Massouh, 1997], or stromal/immunocyte mediators [Pachówka et al., 2011; Wong et al., 2010].

Greater β-AR upregulation and signaling in aging splenocytes *ex vivo* (Fig. 11B) are inconsistent with the age-related increase in SNA. However, degeneration of NA nerves increases the distance for NE diffusion, and therefore reduces ligand availability, which may explain this discrepancy (Fig. 11B). This interpretation is analogous with other types of neurotoxic damage to NA nerves [Tumer et al., 1990; Chatelain et al., 1983]. Also, rising free plasma corticosterone (CORT) levels with age (~70%, 9-19M) [Sabatino et al., 1991] can upregulate β-AR transcriptionally [Kumer and Vrana, 1996; Sabban et al., 2006].

Alternatively, our data agree with reports of age-related alterations in G protein-coupled receptor kinases (GRKs) and β-arrestin expression and activity in liver, vascular smooth muscle and myocardial cells from F344 rats [Kim et al., 2009; Schutzer et al, 2005; Dobson et al., 2003]. Since GRKs, particularly, GRK-2, and β-arrestin are required for $β_2$-AR desensitization through internalization and degradation, our observed increase in β-AR signaling despite increased SNA could also be explained by a deficiency of old splenocytes to internalize β-AR in response to higher NE concentrations. It is not clear from the present study how greater SNA and reduced nerve density interact to affect the extracellular NE concentration at splenocyte neuroeffector junctions. Future studies investigating β-AR down-regulation in aged splenocytes are needed to better understand the observed changes in β-AR expression and signaling. However, $Rilm_{lo}$, which lowers SNA, further augmented β-AR density and signaling in splenocytes from 18M rats, suggesting that β-AR in splenocytes from 18M rats retain the ability to up-regulate in response to reduced NE availability.

Stress-induced effects on body weights in injected rats suggest hypothalamo-pituitary adrenal axis (HPA) and/or SNS activation [Kyrou and Tsigos, 2009]. Our findings are consistent with Uchida et al. [2008] who report chronically elevated circulating corticosterone levels and failure to increase body weights in young male F344 rats receiving 14 days of 2-h restraint stress. In our study there is no supporting evidence for SNS

involvement as there were no stress effects on plasma NE or EPI. However, SNA does not always increase plasma NE levels [Esler et al., 1984], and stress-induced SNA may be transient, returning to baseline before blood collection. Rilm treatment should not remarkably affect stress-induced effects, as sympathetically-mediated reflexes and psychological stressors are still elicited after Rilm treatment [Burke et al., 2010; Esler et al., 2004]. Altered hemostasis may explain the Rilm$_{hi}$-induced increase in spleen weights. Since, the splenic red pulp is a reservoir for blood, vasodilation by Rilm would favor blood accumulation [Kimura et al., 2001; Stewart and McKenzie, 2002]. The negative correlations between spleen weight and NE concentration or content support this hypothesis.

Collectively, our data indicate that, Rilm, or other IR$_1$ agonists that act in the RVLM can reduce SNA and protect NA nerves in the aging spleen. Our data support a role for heightened SNA in NA nerve loss in the aging spleen, and that Rilm can affect NE synthesis. β-AR density and signaling data support normal regulation of postsynaptic events in aging. They also suggest that drugs in this class can affect immune function indirectly by altering splenic SNA. While refinement of the timing of treatment relative to age and drug wash-out studies are needed, our data indicate that reducing central SNA may be a useful strategy for reversing age-related nerve loss. This is a necessary requirement for developing a model to study causal relationships between age-related changes in the SNS and immune system.

Acknowledgments

REFERENCES CITED

Banerjee M, Sanderson JD, Spencer J, Dunn-Walters DK. Immunohistochemical analysis of ageing human B and T cell populations reveals an age-related decline of CD8 T cells in spleen but not gut-associated lymphoid tissue (GALT). Mech Ageing Dev. 2000; 115:85–99. [PubMed: 10854631]

Bellinger DL, Ackerman DK, Felten SY, Felten DL. A longitudinal study of age-related loss of NA nerves and lymphoid cells in the aged rat spleen. Exp Neurol. 1992; 116:295–311. [PubMed: 1350254]

Bellinger, DL.; Madden, KS.; Lorton, D.; ThyagaRajan, S.; Felten, S. Age-related alterations in neural-immune interactions and neural strategies in immunosenescence. In: Ader, R.; Felten, DL.; Cohen, N., editors. Psychoneuroimmunology. Third Edition. Academic Press; San Diego: 2001. p. 113-160.

Bellinger DL, Silva D, Millar AB, Molinaro C, Ghamsary M, Carter J, Lorton D, Lubahn S, ThyagaRajan S. Sympathetic nervous system and lymphocyte proliferation in the Fischer 344 rat spleen: A longitudinal study. Neuroimmunomodulation. 2008a; 15:260–271. [PubMed: 19047803]

Bellinger DL, Millar BA, Perez S, Carter J, Wood C, Thyagarajan S, Molinaro C, Lubahn C, Lorton D. Sympathetic modulation of immunity: Relevance to disease. Cell Immunol. 2008b; 252:27–56. [PubMed: 18308299]

Bellinger DL, Tran L, Kang JI, Lubahn C, Felten, Lorton DL. Age-related changes in noradrenergic sympathetic innervation of the rat spleen are strain dependent. Brain Behav Immun. 2002; 16:247–261. [PubMed: 12009685]

Beluli DJ, Weaver LC. Areas of rostral medulla providing tonic control of renal and splenic nerves. Am J Physiol. 1991; 261:H1687–H1692. [PubMed: 1750526]

Bruban V, Feldman J, Greney H, Dontenwill M, Schann S, Jarry C, Payard M, Boutin J, Scalbert E, Pfeiffer B, Renard P, Vanhoutte P, Bousquet P. Respective contribution of alpha-adrenergic and non-adrenergic mechanisms in the hypotensive effect of imidazoline-like drugs. Br J Pharmacol. 2001; 133:261–266. [PubMed: 11350862]

Burke SL, Head GA. Cardiac and renal baroreflex control during stress in conscious renovascular hypertensive rabbits: effects of rilmenidine. J Hypertens. 2009; 27:132–141. [PubMed: 19145779]

Burke WJ, Li SW, Chung HD, Ruggiero DA, Kristal BS, Johnson EM, Lampe P, Kumar VB, Franko M, Williams EA, Zahm DS. Neurotoxicity of MAO metabolites of catecholamine neurotransmitters: role in neurodegenerative diseases. Neurotoxicology. 2004; 25:101–115. [PubMed: 14697885]

Burke SL, Evans RG, Head GA. Effects of chronic sympatho-inhibition on reflex control of renal blood flow and plasma renin activity in renovascular hypertension. Br J Pharmacol. 2010; 159:438–448. [PubMed: 20015085]

Chatelain P, Robberecht P, Camus JC, De Neef P, Waelbroeck M, Roba J, Christophe J. The adenylate cyclase activity in heart membranes from normotensive and spontaneously hypertensive rats, after chemical sympathectomy, suggests the presence of presynaptic secretin receptors. Eur J Pharmacol. 1983; 93:271–276. [PubMed: 6315454]

Chen KB, Lin AM, Chiu TH. Oxidative injury to the locus coeruleus of rat brain: neuroprotection by melatonin. J Pineal Res. 2003; 35:109–117. [PubMed: 12887654]

Chinta SJ, Andersen JK. Redox imbalance in Parkinson's disease. Biochim Biophys Acta. 2008; 1780:1362–1367. [PubMed: 18358848]

Cohen S, Miller GE, Rabin BS. Psychological stress and antibody response to immunization: a critical review of the human literature. Psychosom Med. 2001; 63:7–18. [PubMed: 11211068]

Cowen T, Thrasivoulou C. Cerebrovascular nerves in old rats reduced accumulation of 5-hydroxytryptamine and loss of nerve fibres. Brain Res. 1990; 513:237–243. [PubMed: 2350693]

Chrousos GP. Stress, chronic inflammation, and emotional and physical well-being: concurrent effects and chronic sequelae. J Allergy Clin Immunol. 2000; 106(5 Suppl):S275–S291. [PubMed: 11080744]

Dampney RA. Functional organization of central pathways regulating the cardiovascular system. Physiol Rev. 1994; 74:323–364. [PubMed: 8171117]

Dardonville C, Rozas I. Imidazoline binding sites and their ligands: an overview of the different chemical structures. Med Res Rev. 2004; 24:639–661. [PubMed: 15224384]

del Rey A, Besedovsky HO, Sorkin E, Da Prada M, Bondiolotti GP. Sympathetic immunoregulation: difference between high- and low-responder animals. Am J Physiol. 1982; 242:R30–R33. [PubMed: 7058928]

Dobson JG Jr, Fray J, Leonard JL, Pratt RE. Molecular mechanisms of reduced beta-adrenergic signaling in the aged heart as revealed by genomic profiling. Physiol Genomics. 2003; 15:142–147. [PubMed: 12902548]

Docherty JR. Age-related changes in adrenergic neuroeffector transmission. Auton Neurosci. 2002; 96:8–12. [PubMed: 11911505]

Dontenwill M, Vonthron C, Greney H, Magnier C, Heemskerk F, Bousquet P. Identification of human I1 receptors and their relationship to alpha 2-adrenoceptors. Ann N Y Acad Sci. 1999; 881:123–134. [PubMed: 10415908]

Dunkley PR, Bobrovskaya L, Graham ME, von Nagy-Felsobuki EI, Dickson PW. Tyrosine hydroxylase phosphorylation: regulation and consequences. J Neurochem. 2004; 91:1025–1043. [PubMed: 15569247]

Ernsberger P. The I1-imidazoline receptor and its cellular signaling pathways. Ann N Y Acad Sci. 1999; 881:35–53. [PubMed: 10415895]

Esler M, Lux A, Jennings G, Hastings J, Socratous F, Lambert G. Rilmenidine sympatholytic activity preserves mental and orthostatic sympathetic response and epinephrine secretion. Arch Mal Coeur Vaiss. 2004; 97:786–792. [PubMed: 15506067]

Esler M, Jennings G, Korner P, Blombery P, Sacharias N, Leonard P. Measurement of total and organ-specific norepinephrine kinetics in humans. Am J Physiol. 1984; 247:E21–E28. [PubMed: 6742187]

Flatmark T. Catecholamine biosynthesis and physiological regulation in neuroendocrine cells. Acta Physiol Scand. 2000; 168:1–17. [PubMed: 10691773]

Fló J, Massouh E. Age-related changes of naive and memory CD4 rat lymphocyte subsets in mucosal and systemic lymphoid organs. Dev Comp Immunol. 1997:443–453. [PubMed: 9397350]

Goldstein DS, McEwen B. Allostasis, homeostats, and the nature of stress. Stress. 2002; 5:55–58. [PubMed: 12171767]

Göthert M, Brüss M, Bönisch H, Molderings GJ. Presynaptic imidazoline receptors. New developments in characterization and classification. Ann N Y Acad Sci. 1999; 881:171–184. [PubMed: 10415912]

Halper JP, Mann JJ, Weksler ME, Bilezikian JP, Sweeney JA, Brown RP, Golbourne T. Beta adrenergic receptors and cyclic AMP levels in intact human lymphocytes: effects of age and gender. Life Sci. 1984; 35:855–863. [PubMed: 6090853]

Jiang D, Fei RG, Pendergrass WR, Wolf NS. An age-related reduction in the replicative capacity of two murine hematopoietic stroma cell types. Exp Hematol. 1992; 20:1216–1222. [PubMed: 1426101]

Jinsmaa Y, Florang VR, Rees JN, Anderson DG, Strack S, Doorn JA. Products of oxidative stress inhibit aldehyde oxidation and reduction pathways in dopamine catabolism yielding elevated levels of a reactive intermediate. Chem Res Toxicol. 2009; 22:835–841. [PubMed: 19388687]

Kim K, Cho SC, Cova A, Jang IS, Park SC. Alterations of epinephrine-induced gluconeogenesis in aging. Exp Mol Med. 2009; 41:334–340. [PubMed: 19307753]

Kimura K, Fusano T, Tanaka Y. A scanning and transmission electron microscopic study of contractile trabecules in the rat spleen. Okajimas Folia Anat Jpn. 2001; 78:187–199. [PubMed: 11915361]

Kin NW, Sanders VM. It takes nerve to tell T and B cells what to do. J Leukoc Biol. 2006; 79:1093–1104. [PubMed: 16531560]

Kumer SC, Vrana KE. The intricate regulation of tyrosine hydroxylase activity and gene expression. J Neurochem. 1996; 67:443–462. [PubMed: 8764568]

Kyrou I, Tsigos C. Stress hormones: physiological stress and regulation of metabolism. Curr Opin Pharmacol. 2009; 9:787–793. [PubMed: 19758844]

McAllen RM, May CN, Shafton AD. Functional anatomy of sympathetic premotor cell groups in the medulla. Clin Exp Hypertens. 1995; 17:209–221. [PubMed: 7735270]

McCarty R. Cardiovascular responses to acute footshock stress in adult and aged Fischer 344 male rats. Neurobiol Aging. 1985; 6:47–50. [PubMed: 4000385]

McCarty R, Pacak K, Goldstein DS, Eisenhofer G. Regulation of peripheral catecholamine responses to acute stress in young adult and aged F-344 rats. Stress. 1997; 2:113–122. [PubMed: 9787260]

Mills PJ, Karnik RS, Dillon E. L-selectin expression affects T-cell circulation following isoproterenol infusion in humans. Brain Behav Immun. 1997; 11:333–342. [PubMed: 9512819]

Monassier L, Greney H, Bousquet P. Chronic treatment with rilmenidine in spontaneously hypertensive rats: differences between two schedules of administration. J Cardiovasc Pharmacol. 2004; 43:394–401. [PubMed: 15076223]

Morgenroth VH 3rd, Boadle-Biber M, Roth RH. Tyrosine hydroxylase: activation by nerve stimulation. Proc Natl Acad Sci U S A. 1974; 71:4283–4287. [PubMed: 4155067]

Parrish DC, Gritman K, Van Winkle DM, Woodward WR, Bader M, Habecker BA. Postinfarct sympathetic hyperactivity differentially stimulates expression of tyrosine hydroxylase and norepinephrine transporter. Am J Physiol Heart Circ Physiol. 2008; 294:H99–H106. [PubMed: 17951370]

Pachówka M, Makula J, Korczak-Kowalska G. Diminished cytokines gene expression in lymphoid organs of healthy aged rats. Cytokine. 2011; 54:24–28. [PubMed: 21215654]

Redwine L, Snow S, Mills P, Irwin M. Acute psychological stress: effects on chemotaxis and cellular adhesion molecule expression. Psychosom Med. 2003; 65:598–603. [PubMed: 12883110]

Reed MC, Lieb A, Nijhout HF. The biological significance of substrate inhibition: a mechanism with diverse functions. Bioessays. 2010; 32:422–429. [PubMed: 20414900]

Reis DJ. Neurons and receptors in the rostroventrolateral medulla mediating the antihypertensive actions of drugs acting at imidazoline receptors. J Cardiovasc Pharmacol. 1996; 27:S11–S18. [PubMed: 8872295]

Sabatino F, Masoro EJ, McMahan CA, Kuhn RW. Assessment of the role of the glucocorticoid system in aging processes and in the action of food restriction. J Gerontol. 1991; 46:B171–179. [PubMed: 1890278]

Sabban EL, Liu X, Serova L, Gueorguiev V, Kvetnansky R. Stress triggered changes in gene expression in adrenal medulla: transcriptional responses to acute and chronic stress. Cell Mol Neurobiol. 2006; 26:845–856. [PubMed: 16691439]

Schutzer WE, Reed JF, Mader SL. Decline in caveolin-1 expression and scaffolding of G protein receptor kinase-2 with age in Fischer 344 aortic vascular smooth muscle. Am J Physiol Heart Circ Physiol. 2005; 288:H2457–64. [PubMed: 15626685]

Stewart IB, McKenzie DC. The human spleen during physiological stress. Sports Med. 2002; 32:361–369. [PubMed: 11980500]

Spengler RN, Allen RM, Remick DG, Strieter RM, Kunkel SL. Stimulation of alpha-adrenergic receptor augments the production of macrophage-derived tumor necrosis factor. J Immunol. 1990; 145:1430–1434. [PubMed: 2166759]

Staehelin M, Müller P, Portenier M, Harris AW. Beta-adrenergic receptors and adenylate cyclase activity in murine lymphoid cell lines. J Cyclic Nucleotide Protein Phosphor Res. 1985; 10:55–64. [PubMed: 2984265]

Stirling DP, Stys PK. Mechanisms of axonal injury: internodal nanocomplexes and calcium deregulation. Trends Mol Med. 2010; 16:160–170. [PubMed: 20207196]

Szabo B. Imidazoline antihypertensive drugs: a critical review on their mechanism of action. Pharmacol Ther. 2002; 93:1–35. [PubMed: 11916539]

ThyagaRajan S, Madden KS, Stevens SY, Felten DL. Restoration of splenic noradrenergic nerve fibers and immune reactivity in old F344 rats: a comparison between L-deprenyl and L desmethyldeprenyl. Int J Immunopharmacol. 2000; 22:523–536. [PubMed: 10785549]

Tsai H, Pottorf WJ, Buchholz JN, Duckles SP. Adrenergic nerve smooth endoplasmic reticulum calcium buffering declines with age. Neurobiol Aging. 1998; 19:89–96. [PubMed: 9562509]

Tumer N, Houck WT, Roberts J. Effect of age on upregulation of the cardiac adrenergic beta receptors. J Gerontol. 1990; 45:B48–B51. [PubMed: 1968920]

Uchida S, Nishida A, Hara K, Kamemoto T, Suetsugi M, Fujimoto M, Watanuki T, Wakabayashi Y, Otsuki K, McEwen BS, Watanabe Y. Characterization of the vulnerability to repeated stress in Fischer 344 rats: possible involvement of microRNA-mediated down-regulation of the glucocorticoid receptor. Eur J Neurosci. 2008; 27:2250–2261. [PubMed: 18445216]

Wallace LJ. A small dopamine permeability of storage vesicle membranes and end product inhibition of tyrosine hydroxylase are sufficient to explain changes occurring in dopamine synthesis and storage after inhibition of neuron firing. Synapse. 2007; 61:715–723. [PubMed: 17559092]

Wong CP, Magnusson KR, Ho E. Aging is associated with altered dendritic cells subset distribution and impaired proinflammatory cytokine production. Exp Gerontol. 2010; 45:163–169. [PubMed: 19932744]
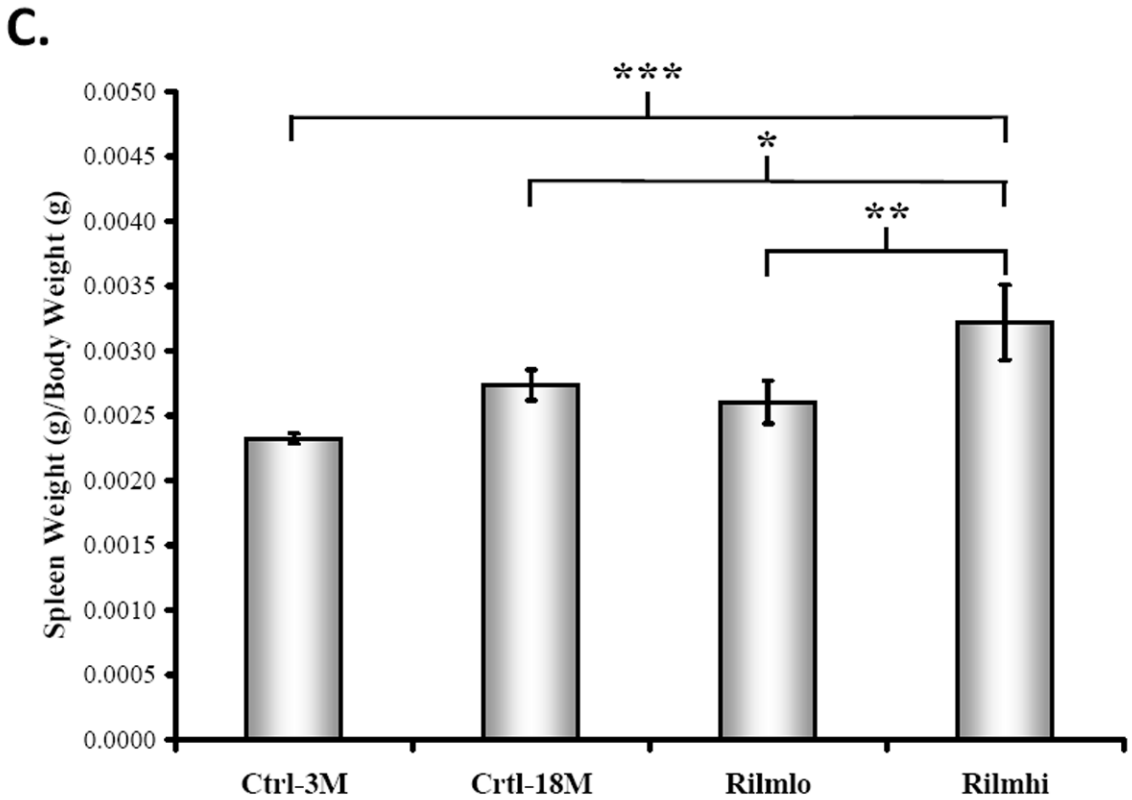
A.

B.

C.
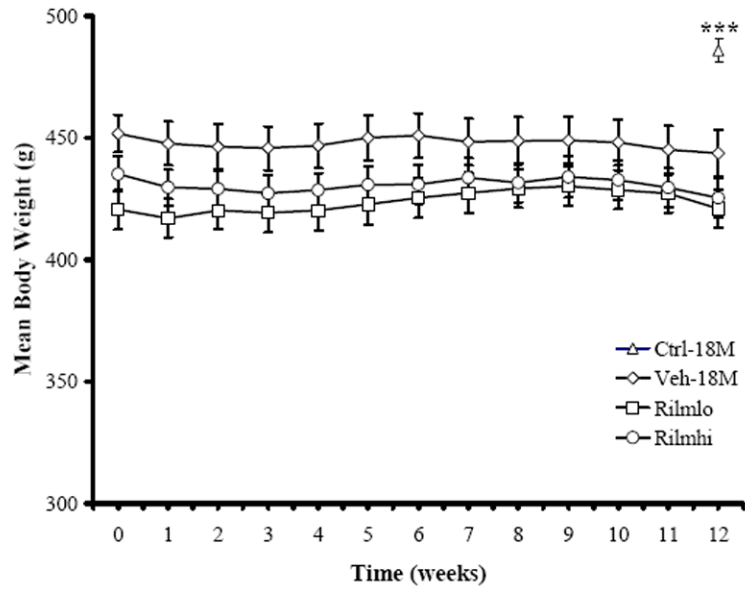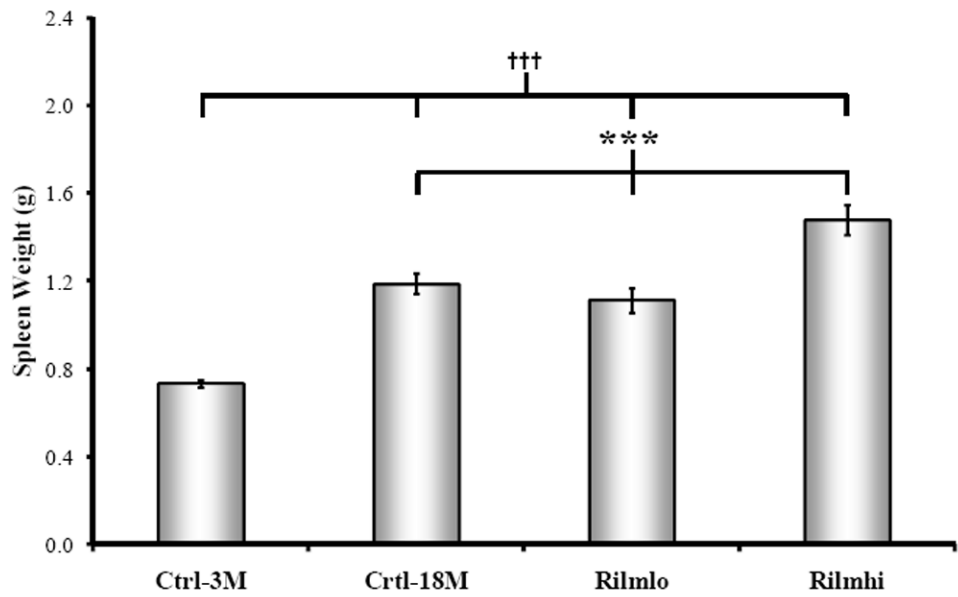
Fig. 1. Mean Body, Spleen and Normalized Spleen Weights over the Time Course of the Experiment

The effect of age and 90-day treatment with control (Ctrl-18M), vehicle treatment (Veh-18M), and low- or high-dose rilmenidine (Rilm$_{lo}$ or Rilm$_{hi}$, respectively) on mean body (**A.**) and spleen weight (**B.**) expressed as means ($\pm$ SEM) in grams (g), and on spleen weight per body weights expressed in g per g (**C.**) in F344 male rats. **A.** All treatment groups maintained, but did not gain weight; Ctrl-18M rats weighed significantly more than all other age-matched treatment groups (***, $p<0.001$). There was no effect of chronic drug treatment on mean body weight over the 90-day period. Ctrl-18M, $\diamondsuit$; Rilm$_{lo}$, $\square$; Rilm$_{hi}$, $\triangle$. **B.** There was a significant effect of age on spleen weight such that all 18M groups were greater than Ctrl-3M rats (†††, $p<0.001$), and treatment with Rilm$_{hi}$, further increased (***, $p<0.001$) mean spleen weight compared with Ctrl-18 and Rilm$_{lo}$. **C.** Treatment with Rilm$_{hi}$ significantly increased spleen weight per body weight compared with all other treatment groups (Ctrl-3M: ***, $p<0.001$; Ctrl-18M: *, $p<0.05$; Rilm$_{lo}$: **, $p<0.01$). Low and high-dose rilmenidine, Rilm$_{lo}$ and Rilm$_{hi}$, respectively; 3- or 18-month-old controls, Ctrl-3M or Ctrl-18M, respectively. Ctrl-3M, $n=14$; Ctrl-18M, $n=22$; Rilm$_{lo}$ or Rilm$_{hi}$, $n=12$.
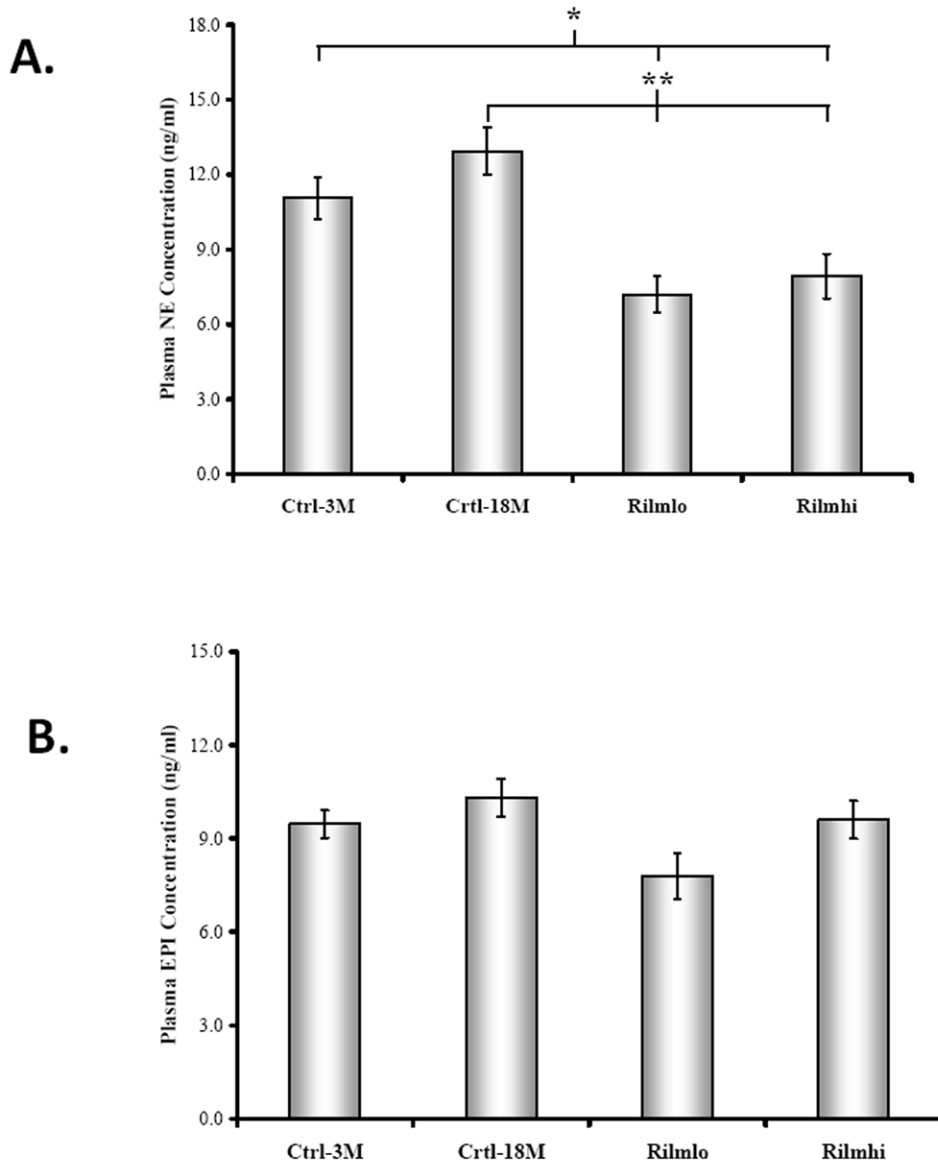
Fig. 2. Effect of Rilmenidine on Circulating Catecholamines
The effect of rilmenidine treatment on mean plasma norepinephrine (NE) and epinephrine (EPI) concentrations (**A. and B.**, respectively) ± SEM expressed in ng/ml. Both doses of rilmenidine over the 90-day period significantly reduced plasma NE (**A.**), but not EPI (**B.**), concentrations compared with Ctrl-3M and Ctrl-18M (*, $p<0.05$ and **, $p<0.01$, respectively). Low and high-dose rilmenidine, $Rilm_{lo}$ and $Rilm_{hi}$, respectively; young, 3-month-old controls, Ctrl-3M; old, 18-month-old controls, Ctrl-18M). Ctrl-3M, $n=14$; Ctrl-18M, $n=22$; $Rilm_{lo}$ or $Rilm_{hi}$, $n=12$).
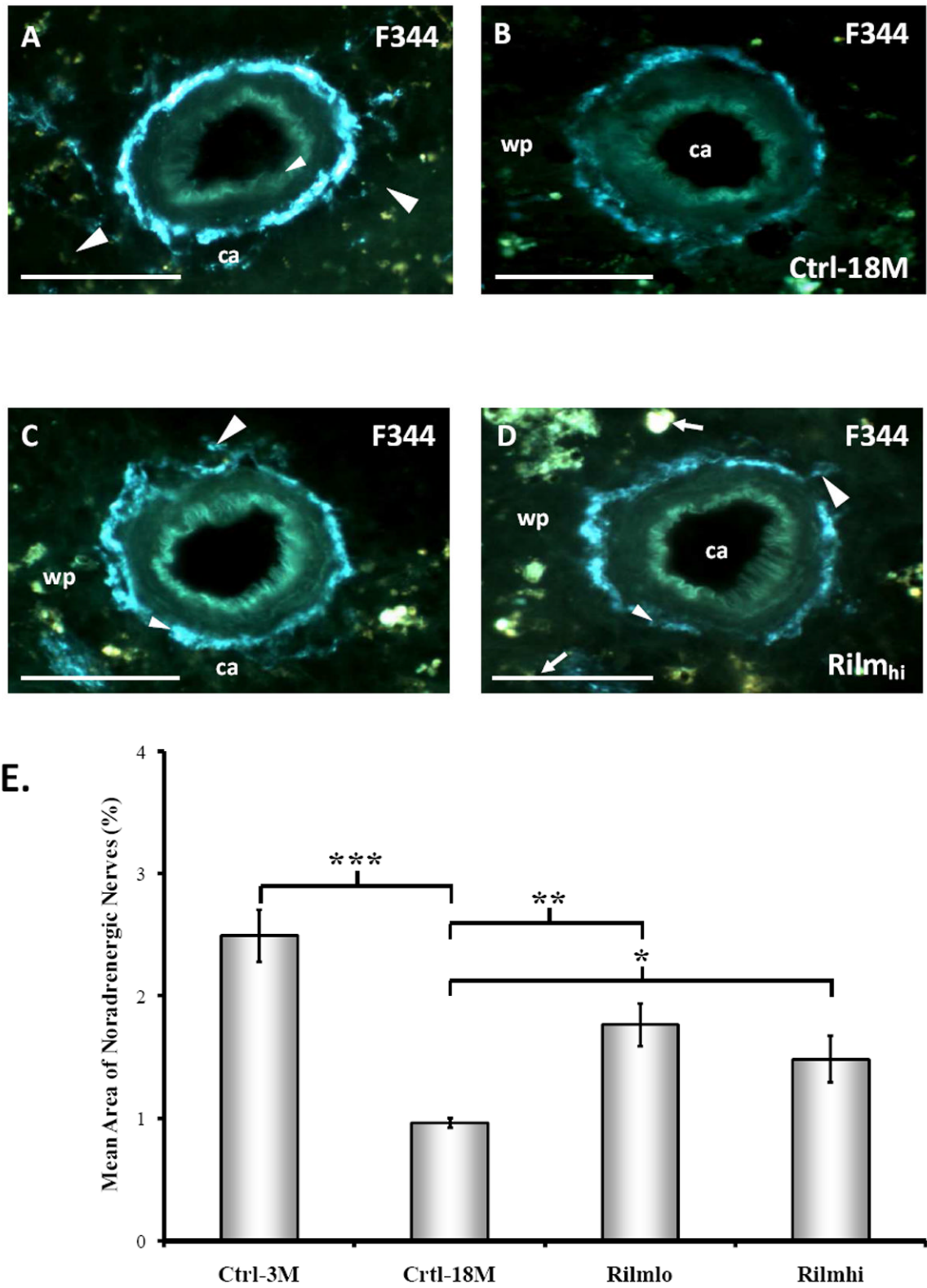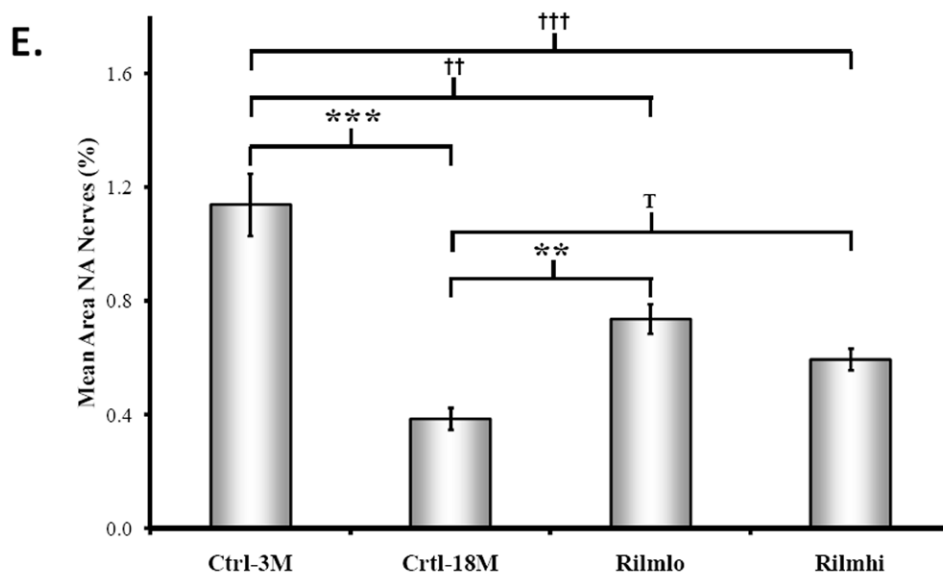
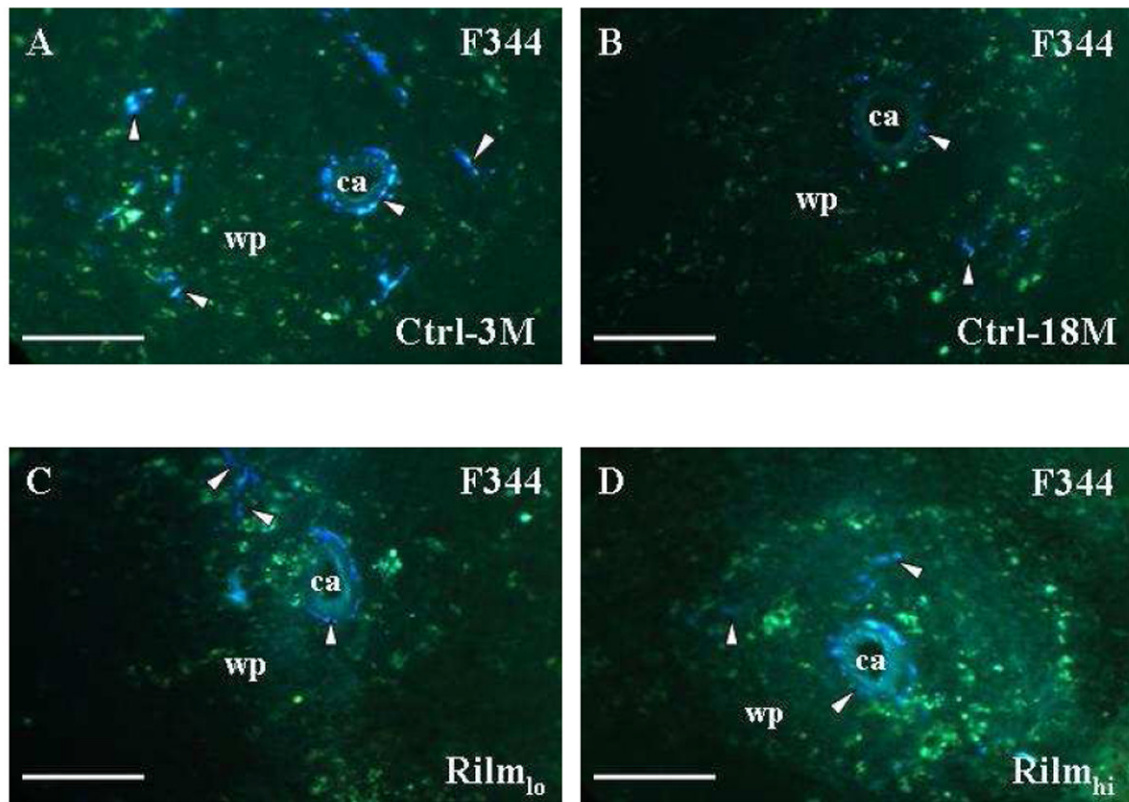**Fig. 3. Effect of Rilmenidine on Splenic NA Innervation at the Hilus**

Fluorescence histochemistry for catecholamines demonstrates abundant fluorescent linear and punctate NA nerve profiles surrounding the central arteriole (ca) in the white pulp (wp) (large arrowheads) in the hilar region of the spleen in 3-month-old F344 rats (Ctrl-3M) (**A.**). At 18 months of age (Ctrl-18M) (**B.**), the density of fluorescent nerves along the central arteriole decline, an effect partially reversed by low- and high-dose rilmenidine treatment (Rilm$_{lo}$ (**C.**) and Rilm$_{hi}$ (**D.**), respectively. Morphometric analysis of fluorescent profiles (**E.**) expressed as percent mean area is consistent with qualitative findings, showing an age-related loss of fluorescent nerves (***, $p < 0.001$) that is attenuated by low- or high-dose rilmenidine treatment (Rilm$_{lo}$: **, $p < 0.001$; Rilm$_{hi}$,*, $p < 0.05$). Low and high-dose rilmenidine, Rilm$_{lo}$ and Rilm$_{hi}$, respectively; young, 3-month-old controls, Ctrl-3M; old, 18-month-old controls, Ctrl-18M). **A-D.** Glyoxylic acid fluorescence histochemistry. In all photomicrographs, the large arrowheads demonstrate nerve profiles in the parenchyma of the white pulp. The arrows and small arrowheads indicate yellow autofluorescent cells and the internal elastic lamina of the central arteriole, respectively. Calibration bar = 100 μm.

Fig. 4. Effect of Rilmenidine on Splenic NA Innervation Distal to the Hilus
Distal to the hilus, fluorescence histochemistry for catecholamines demonstrates fluorescent linear and punctate NA nerve profiles surrounding the central arteriole (ca) in the white pulp (wp) (arrowheads) of the spleen in 3-month-old F344 rats (Ctrl-3M) (**A.**). In this region of the spleen, the white pulps are smaller, central arterioles have a smaller diameter and there are fewer NA nerve surrounding the arterioles compared with the hilar region. However, the

compartmentation of nerves is comparable to the hilar region. At 18 months of age (Ctrl-18M) (**B.**), the density of fluorescent nerves along the central arteriole decline, an effect partially reversed by low- and high-dose rilmenidine treatment ($Rilm_{lo}$ (**C.**) and $Rilm_{hi}$ (**D.**), respectively. Morphometric analysis of fluorescent profiles (**E.**) expressed as percent mean area is consistent with qualitative findings, showing an age-related loss of fluorescent nerves (Ctrl-18M vs. Ctrl-3M: ***, $p<0.001$) that is attenuated by low- or high-dose rilmenidine treatment ($Rilm_{lo}$ or $Rilm_{hi}$ vs. Ctrl-18M: **, $p<0.01$ or **T**, $p<0.1$, respectively; $Rilm_{lo}$ or $Rilm_{hi}$ vs. Ctrl-3M: †, $p<0.01$ or ††, $p<0.001$). Low and high-dose rilmenidine, $Rilm_{lo}$ and $Rilm_{hi}$, respectively; 3- or 18-month-old controls, Ctrl-3M or Ctrl-18M, respectively). **A-D.** Glyoxylic acid fluorescence histochemistry. Calibration bar = 100 μm.
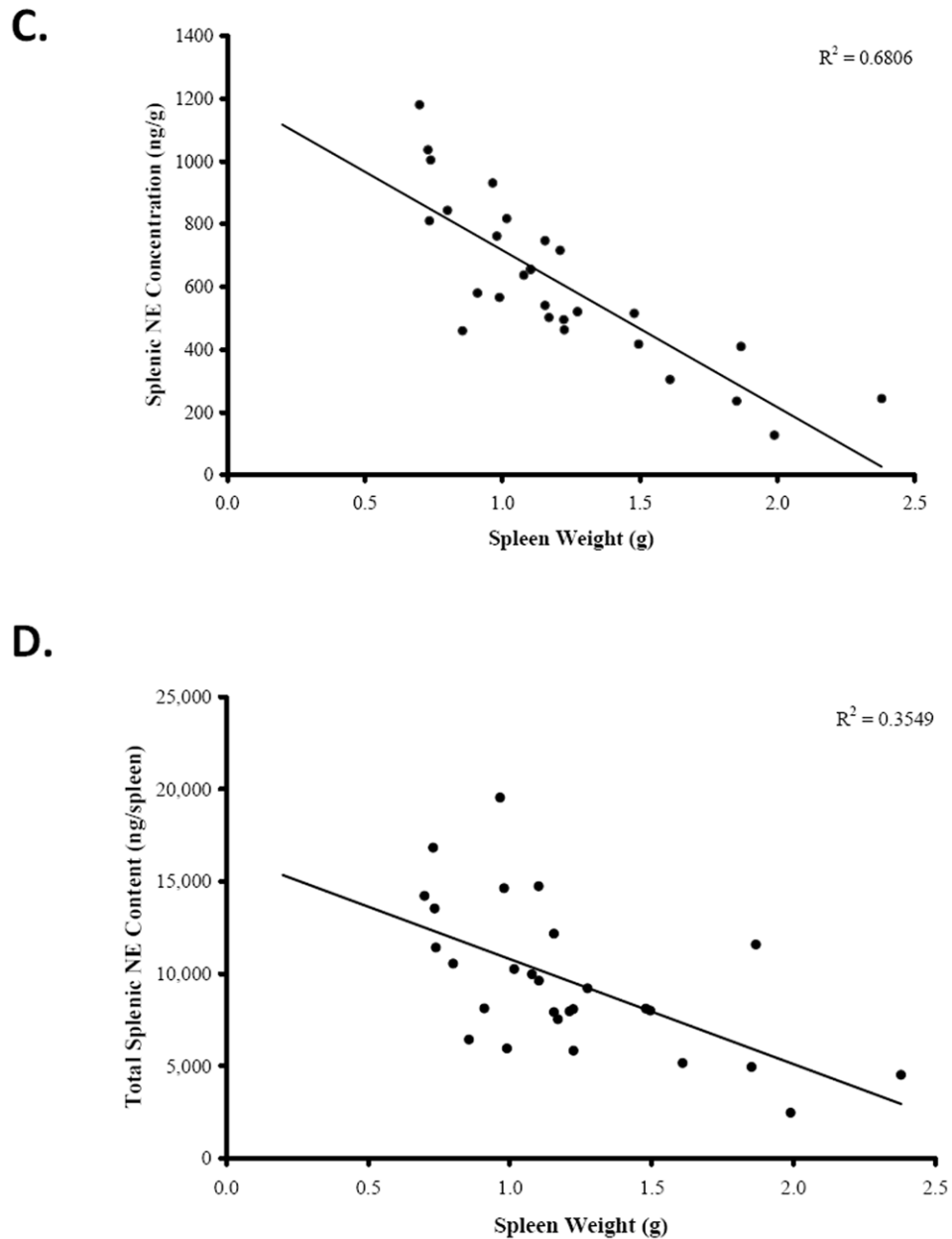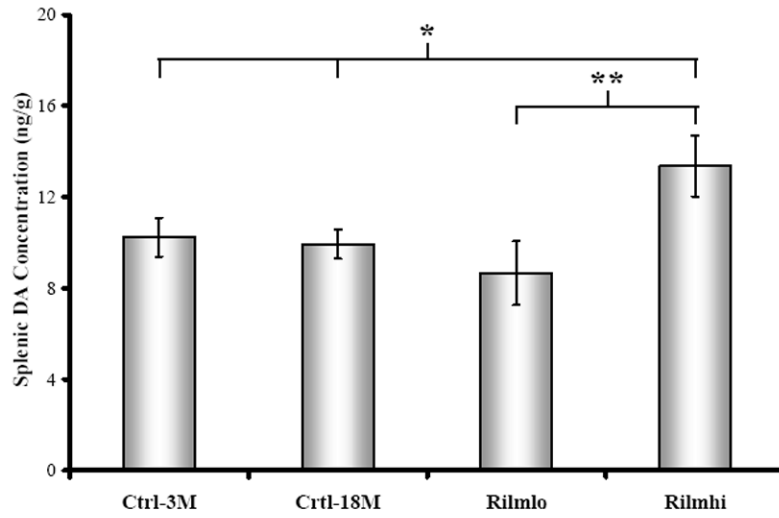
A.

B.

Perez et al.

C.

R² = 0.6806

D.

R² = 0.3549
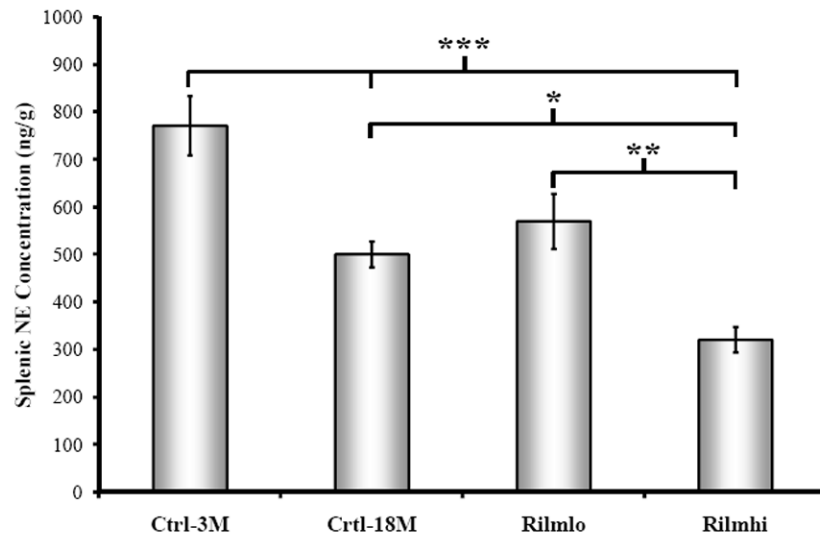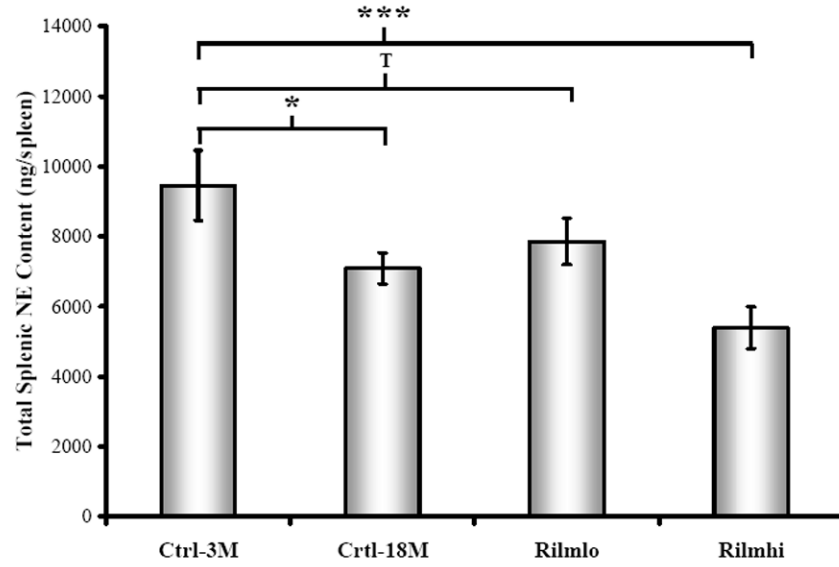
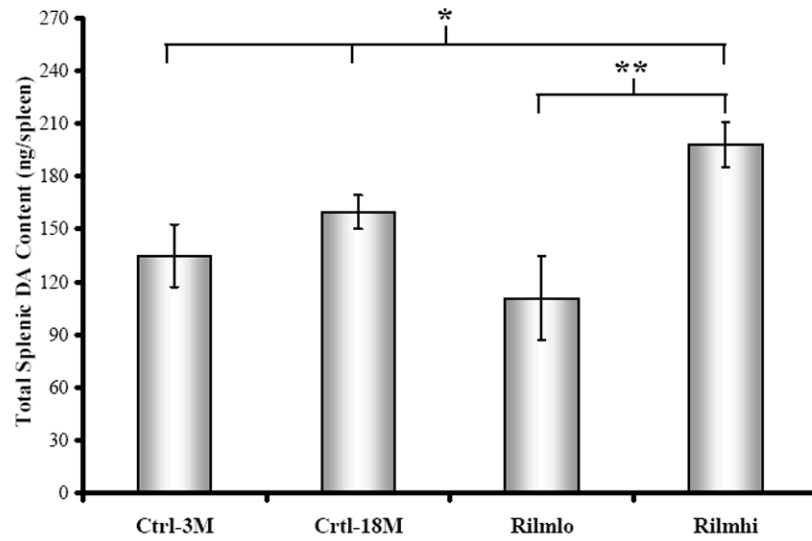**Fig. 5. Rilmenidine and Splenic NE Content and Concentration**
Mean total splenic NE concentrations (expressed as ng/gm wet weight ± SEM) (**A.**) and splenic NE content (expressed as ng/spleen ± SEM) (**B.**) in 3M and 18M controls, and rats treated with low- or high-dose rilmenidine treatment (Ctrl-3M, Ctrl-18M, $Rilm_{lo}$, and $Rilm_{hi}$, respectively). Splenic NE concentration (**A.**) was reduced with advancing age (Ctrl-3M vs. Ctrl- 18M: ***, $p<0.001$), an effect augmented by high-dose rilmenidine treatment ($Rilm_{hi}$) (Ctrl-3M or Ctrl-18 vs. Rilmhi: *, $p<0.05$ or ***, $p<0.001$, respectively). Splenic NE concentration also was lower in Rilmhi than the $Rilm_{lo}$ group (**, $p<0.01$). Similarly, Total NE content in the spleen (**B.**) was diminished in old (Ctrl- 18M) or $Rilm_{lo}$ compared with young (Ctrl-3M) rats (*, $p<0.05$ or ***, $p<0.001$, respectively), with a trend for lower levels in $Rilm_{hi}$ compared with Ctrl-3M (**T**, $p<0.1$). Splenic NE concentration (**C.**)

and content (**D.**) were negatively correlated with spleen weight (R^2=0.68 and 0.35, respectively). Ctrl-3M, n=13; Ctrl-18M, n=23; $Rilm_{lo}$ or $Rilm_{hi}$, n=11
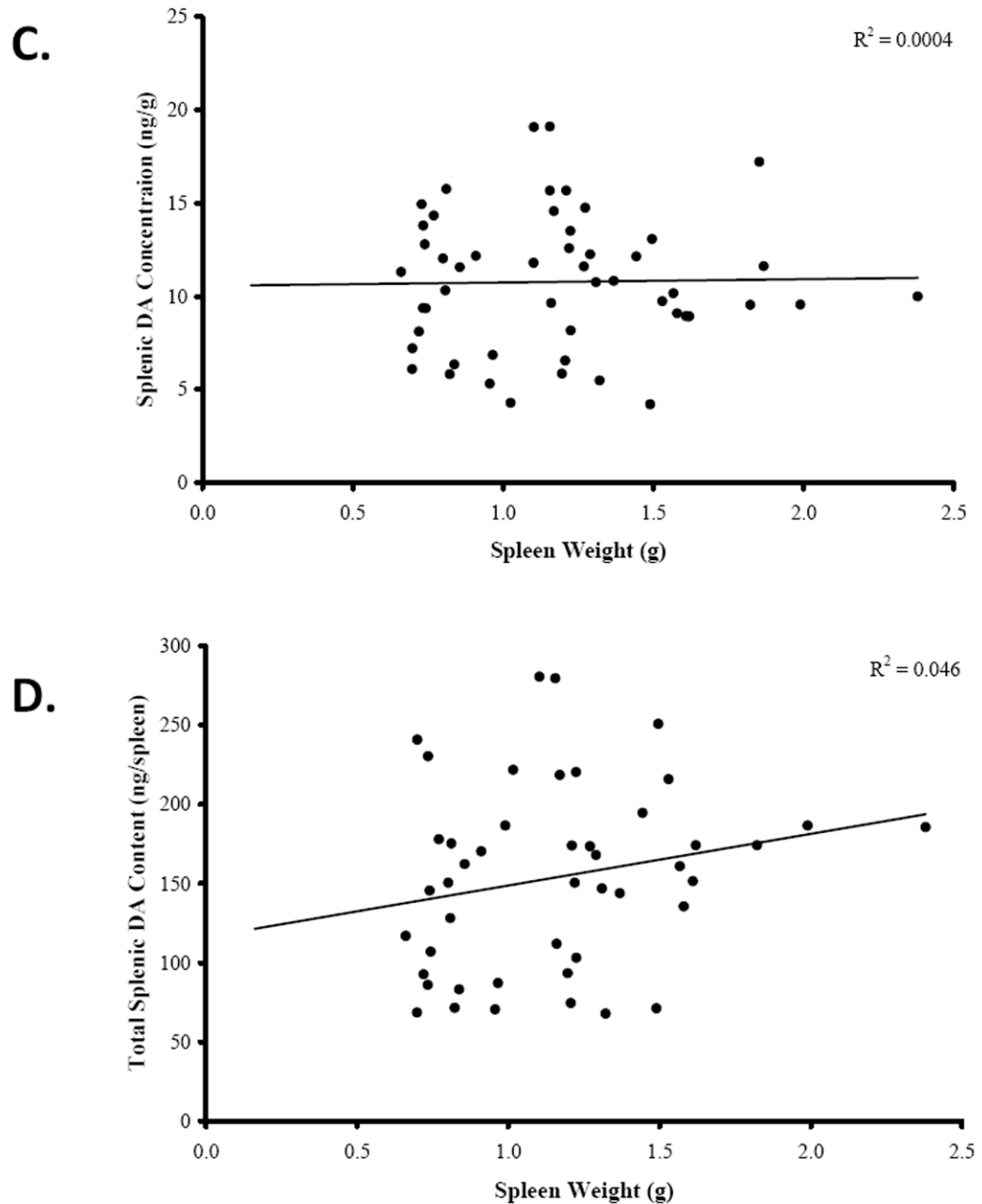
A.

B.

Fig. 6. Rilmenidine and Splenic DA Content and Concentration
Mean total splenic DA concentrations (expressed as ng/gm wet weight ± SEM) (**A.**) and splenic DA content (expressed as ng/spleen ± SEM) (**B.**) in 3M and 18M controls, and rats treated with low- or high-dose rilmenidine treatment (Ctrl-3M, Ctrl-18M, $Rilm_{lo}$, and $Rilm_{hi}$, respectively). There was no effect of age or $Rilm_{lo}$ on splenic DA concentration (**A.**) or content (**B.**); however, $Rilm_{hi}$ significantly increased splenic DA concentration (*,) (A.) and content (**B.**) compared with the other treatment groups (Ctrl-3M or Ctrl-18M: *, $p<0.05$; $Rilm_{lo}$: **, $p<0.01$). Neither splenic DA concentration (**C.**) nor content (**D.**) were correlated with spleen weight ($R^2=0.0004$ and 0.046, respectively). Ctrl-3M, $n=13$; Ctrl-18M, $n=23$; $Rilm_{lo}$ or $Rilm_{hi}$, $n=11$
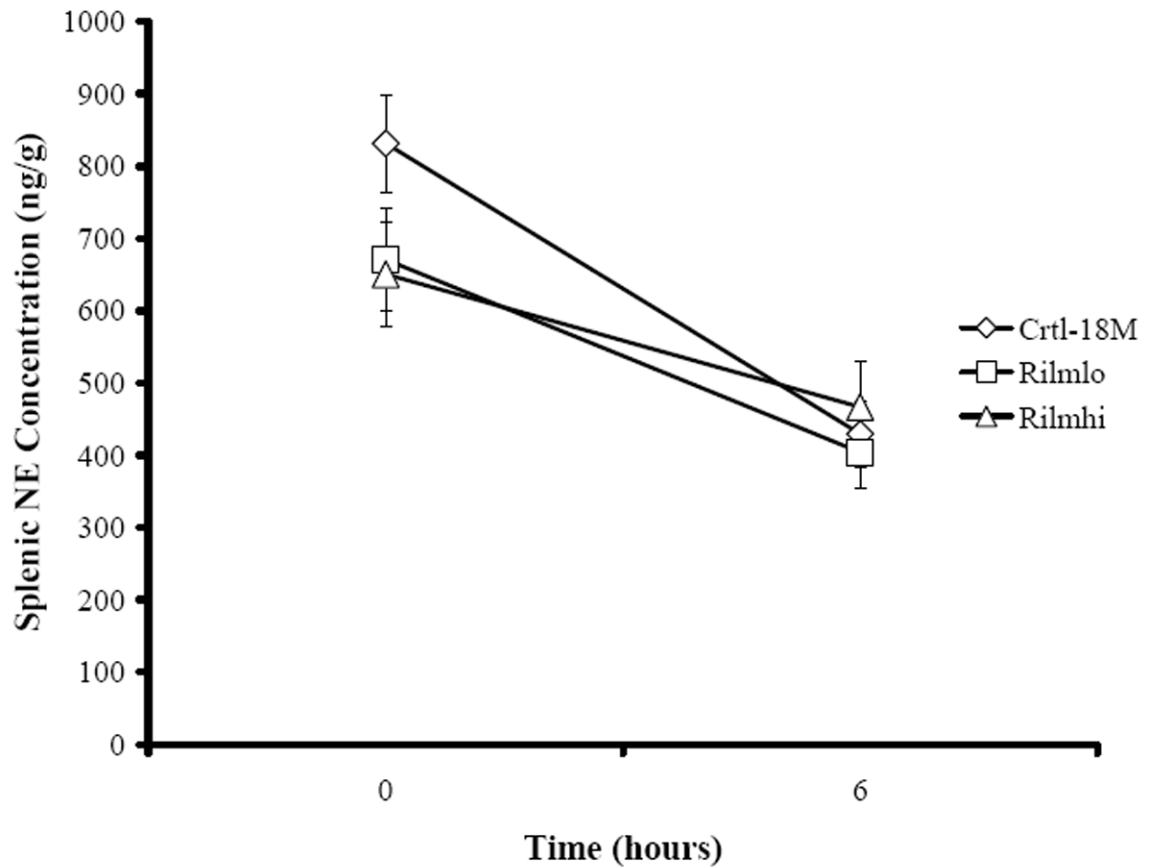
Fig. 7. Effect of Rilmenidine on NE Turnover
The effect of rilmenidine or control on the mean splenic NE concentrations 0 and 6 hours post-injection with αMPT to inhibit NE synthesis is shown. Ninety-day treatment with low- or high-dose rilmenidine (Rilm$_{lo}$, □ or Rilm$_{hi}$, △, respectively) slowed the rate of decline in splenic NE concentration over the 6-hour period compared with age-matched controls (Ctrl-18M, ◇). Data are expressed in ng/g/hr vs. time and each group represents an *n* of 12 rats.
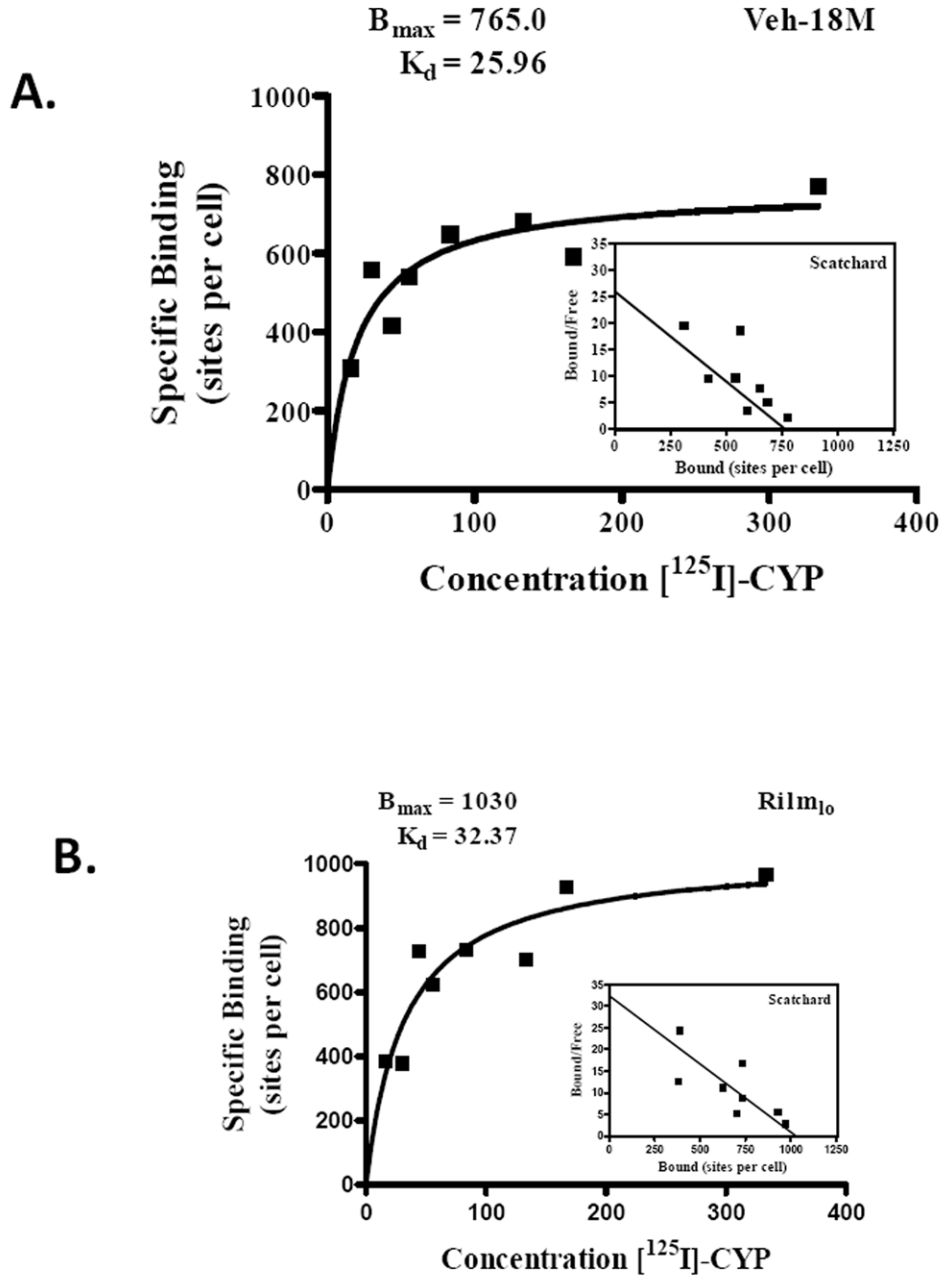
Fig. 8. Effect of Rilmenidine on β-AR Binding in Splenocytes
Specific binding and Scatchard plots of (-)-[^{125}I]cyanopindolol ([^{125}I]CYP) in whole spleen cells from age-matched vehicle- (Veh-18M) and low-dose rilmenidine (Rilm$_{lo}$)-treated rat (**A.** and **B.**, respectively). Spleen cells were incubated under equilibrium binding conditions at 37 °C with ICYP (0.9-220 pM) for 60 min, then the reaction was stopped and the radioactivity was quantified by gamma scintillation spectrometry. Specific binding and plots represent means of duplicate determinations of specific (■) binding. cpm, counts/min. Each group represents an *n* of 6 rats.
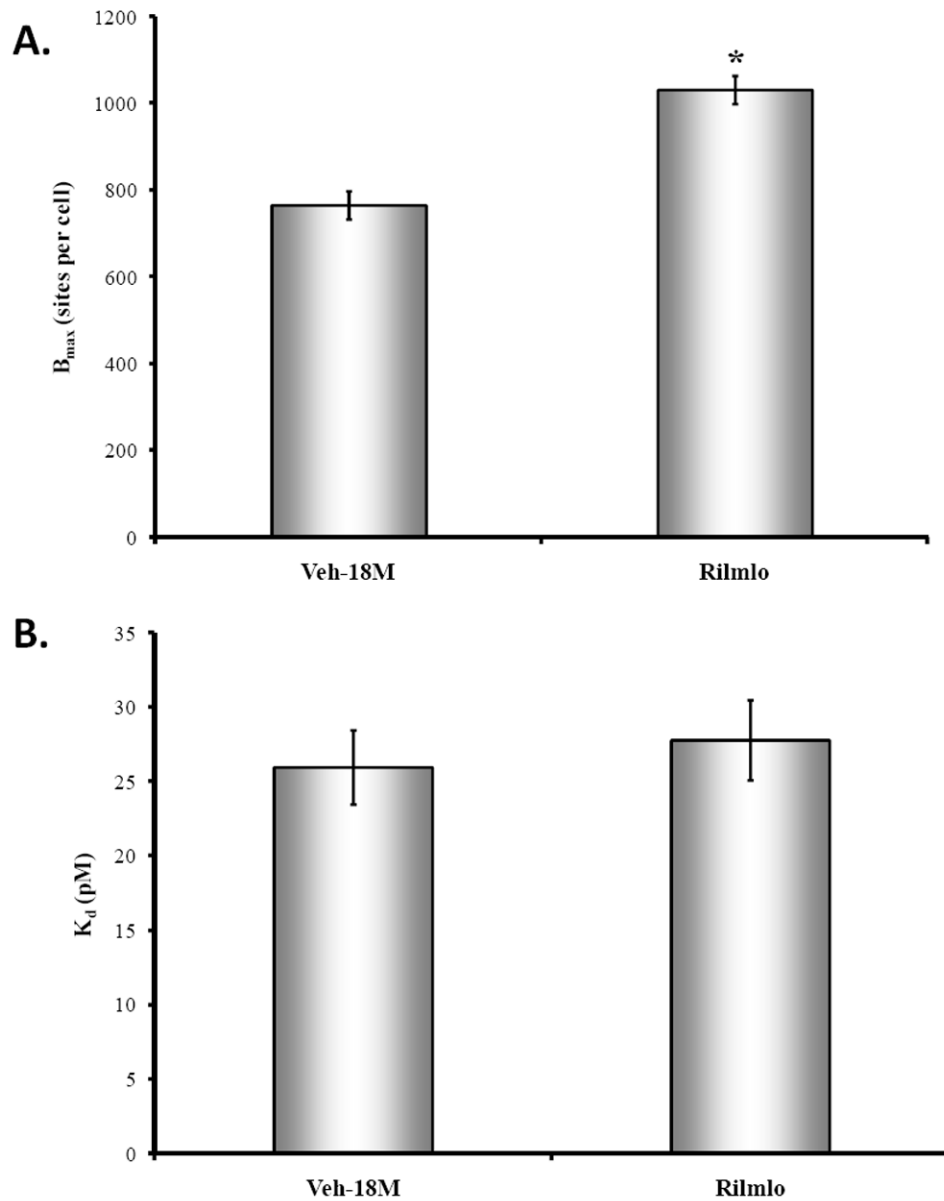
Fig. 9. Mean B_{max} and K_D in $Rilm_{lo}$ and Veh-18M
The mean density of β-AR expressed as sites/cell (A) and K_D (B) on spleen cells from vehicle-treated (Veh-18M) and low-dose rilmenidine ($Rilm_{lo}$)-treated rats (*n* of 6 per group) demonstrates that chronic treatment with $Rilm_{lo}$ significantly increased β-AR expression on splenocytes (*, $p < 0.05$) without affecting K_D. Mean values were calculated from the B_{max} and K_D determined form specific binding curves generated for each rat from each treatment group.
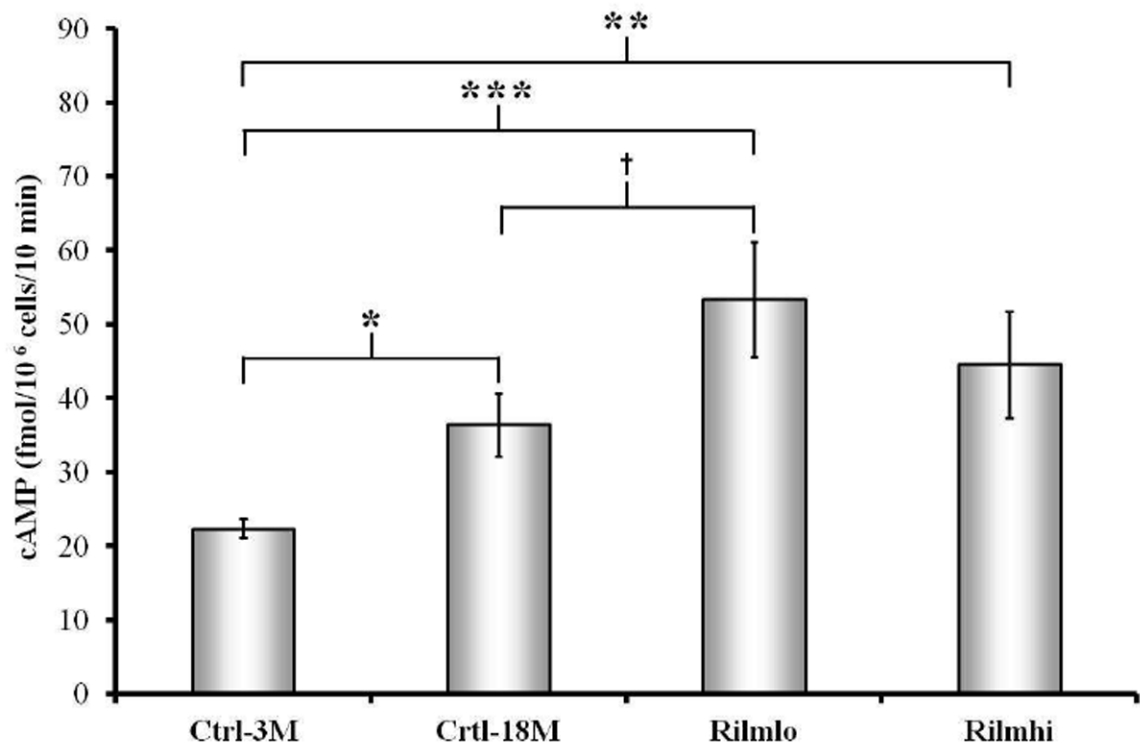
Fig. 10. Effect of Rilmenidine on Splenocyte cAMP Production
Isoproterenol-stimulated cAMP production in spleen cells *in vitro* was increased in all 18M groups compared with young controls (Ctrl-3M) (Ctrl-18M: *, $p<0.05$; Rilm$_{lo}$: ***, $p<0.001$; Rilm$_{hi}$: **, $p<0.01$), and Rilm$_{lo}$ values were greater than in Ctrl-18M rats (†, $p<0.05$). Data are expressed in fmol/10^6 cells/10 min. Low and high-dose rilmenidine, Rilm$_{lo}$ and Rilm$_{hi}$, respectively; 3-month-old controls, Ctrl-3M; 18-month-old controls, Ctrl-18M). Ctrl-3M, $n=11$; Ctrl-18M, $n=19$; Rilm$_{lo}$, $n=12$; Rilm$_{hi}$, $n=11$.
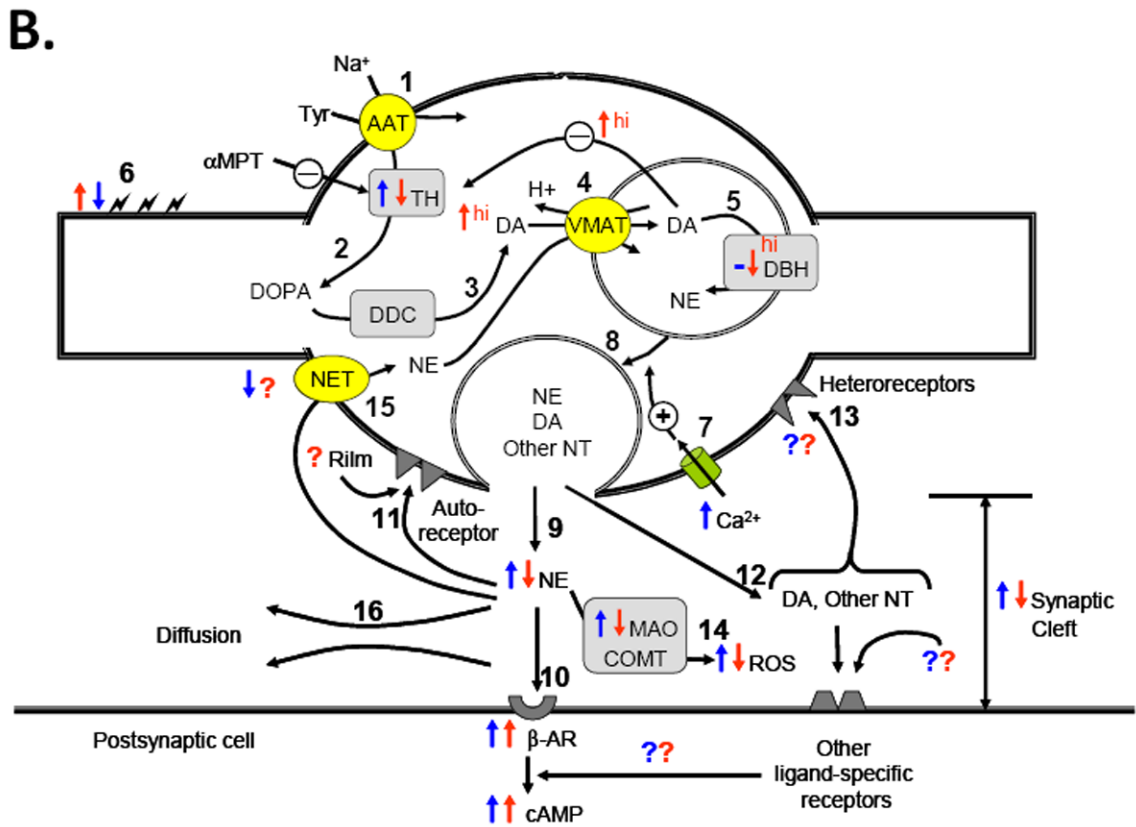
A.
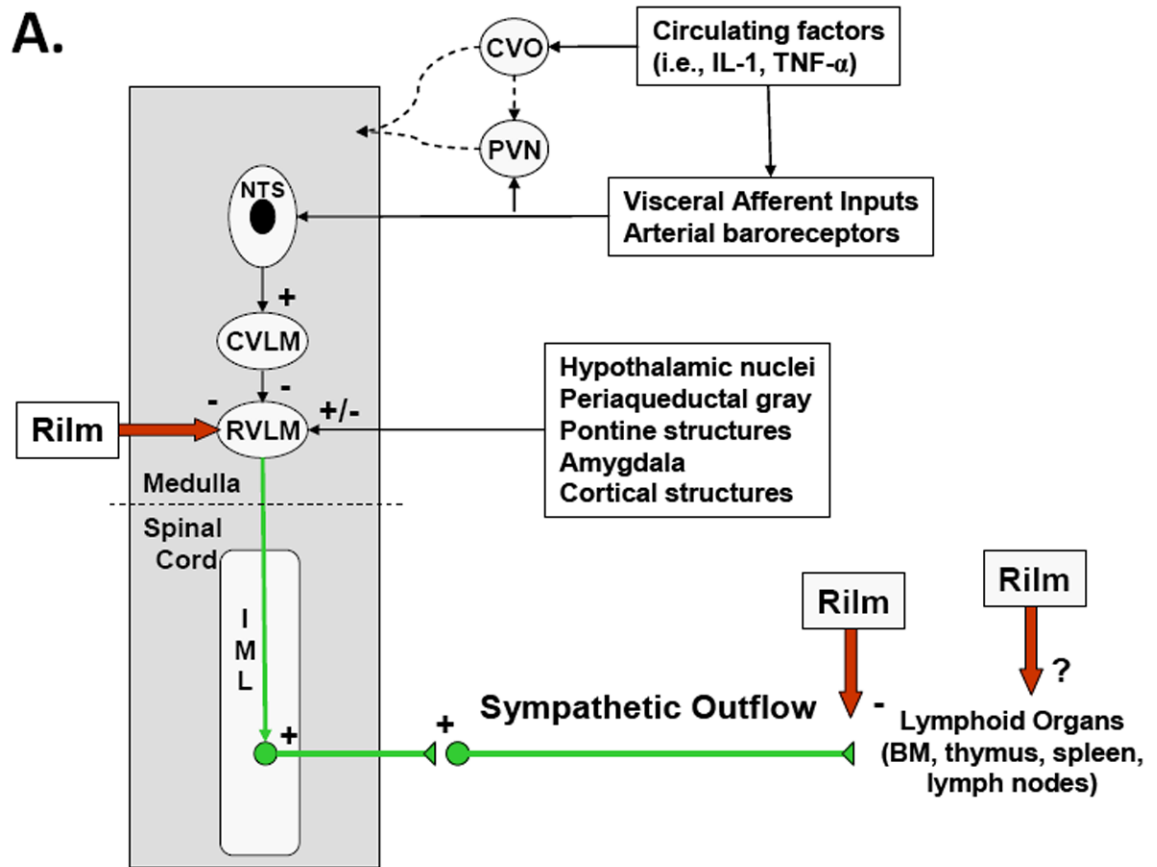
Fig. 11. Rilmenidine Modifies the Activity of the RVLM to Affect Sympathetic Outflow to the Spleen

General schematic diagram identifying potential central neural sites involved in the regulation of sympathetic outflow to lymphoid organs (**A.**). The rostral ventrolateral medulla (RVLM) is a site of a complex convergence of descending and ascending neural inputs. The excitatory drive from the RVLM is intrinsically generated, but can be modulated by excitatory and inhibitory inputs from other regions of the central nervous system (e.g., pons, hypothalamus and amygdala) that process a wide array of sensory stimuli (including baroceptive, nociceptive, and immunological) and participate in stress, emotion and behavioral responses. The neurons of the RVLM drive sympathetic outflow by synapsing onto preganglionic neurons in the intermediolateral cell column (IML) to modulate the activity of postganglionic neurons that supply lymphoid organs. Inflammatory cytokines, such as interleukin-1 (IL-1) and tumor necrosis factor-alpha (TNF-α) act on the circumventricular organ (CVO) and visceral afferent fibers to influence the activity of the paraventricular nucleus (PVN) and nucleus tractus solitarius (NTS), which in turn, modulates the activity of the RVLM indirectly via input to the caudal ventrolateral medulla (CVLM). Rilmenidine (Rilm) acts on IR_1 and α_2-AR primarily in RVLM to inhibit the sympathoexcitatory neurons that impinge on the 2-neuron sympathetic chain that supplies the spleen. (Modified from Dampney, 1994). **B.** Schematic diagram of a NA junction in the spleen illustrating the biosynthesis of NE, and NA neurotransmission. Proposed effects of age (shown in blue) and rilmenidine (shown in red) on these processes are indicated and described in the text. **1.** Tyrosine (Tyr) is transported into the NA varicosity by a sodium-dependent carrier (AAT). **2.** Tyr is converted to DOPA via the rate-limiting enzyme, tyrosine hydroxylase (TH). **3**. Decarboxylation by dopamine decarboxylase (DDC) forms DA. **4.** DA is transported into the vesicle by the vesicular monoamine transporter (VMAT).

This same carrier transports NE into these granules. **5.** DA is converted to NE in the vesicle by dopamine-β-hydroxylase (DBH). **6.** Physiological release of transmitter occurs via tonic firing of the nerve (✗). **7.** Action potentials open voltage-sensitive calcium channels and increase intracellular calcium (Ca^{2+}). A decline in Ca^{2+} ATPase activity in smooth endoplasmic reticulum can increase stimulation-evoke NE release in older NA nerves (blue arrow). **8.** Fusion of vesicles with the surface membrane results in expulsion of NE, DA, other cotransmitters, as well as DBH. **9.** After release, NE diffuses into the cleft. **10.** NE binds with postsynaptic receptors, predominantly β_2-AR in lymphocytes, which increases intracellular cAMP. **11.** NE binds with presynaptic autoreceptors (α_2-AR), providing feedback regulation of NE release. **12.** Cotransmitters (NT) released with NE interact with presynaptic (heteroreceptors) and postsynaptic receptors; signaling via cotransmitters can affect β-AR mediated signaling. **13.** Binding with heteroreceptors also regulates NE release. **14.** NE degradation in the cleft occurs by monoamine oxidase (MAO) and catechol-O-methyltransferase (COMT), which increases reactive oxygen species (ROS). **15.** NE is transported back into the terminal by the NE transporter (NET). **16.** NE diffuses away from the cleft and into the bloodstream.

TABLE 1

Effect of Chronic Rilmenidine on Splenic NE Turnover Rate

Treatment Group	Initial Levels (ng/g±SEM)	n^a	Rate Constant of NE Loss[b] k(h)	n^c	Turnover Rate[d] (ng/g/h)	Turnover Time[e] (h)	Fold Change in Turnover Rate from Veh-15M[f]
Ctrl-18M	584.9 ± 50.9	15	0.42	7	246.1	2.4	3.6↑
Rilmlo	483.3 ± 53.7	16	0.34	8	165.9	2.9	2.4↑
Rilmhi	364 ± 51.6	13	0.1	7	45.1	10.0	0.7↓

[a] Number of αMPT- or vehicle-treated rats at time 0

[b] Calculated from the slope of decline of log NE content

[c] Number of αMPT rats sacrificed at time 6

[d] NE synthesized and degraded per gram spleen tissue per hour

[e] Time required to synthesize the steady-state tissue pool of NE

[f] Calculations based on turnover rates from vehicle-treated 15M rats reported in Bellinger et al 2008c